

Submitted to: *New J. Phys.*

Signatures of a localizable bath in the memory kernel of a generalized quantum master equation

Nathan Ng

Department of Physics, University of California, Berkeley, CA 94720, USA

Eran Rabani

Department of Chemistry, University of California, Berkeley, CA 94720, USA
Materials Sciences Division, Lawrence Berkeley National Laboratory, Berkeley, CA 94720, USA

The Sackler Center for Computational Molecular and Materials Science, Tel Aviv University, Tel Aviv 69978, Israel

Abstract. We study the properties of the Nakajima-Zwanzig memory kernel for a qubit immersed in a many-body localized (i.e. disordered and interacting) bath. We argue that the memory kernel decays as a power law in both the localized and ergodic regimes, and show how this can be leveraged to extract $t \rightarrow \infty$ populations for the qubit from finite time ($Jt \leq 10^2$) data in the thermalizing phase. This allows us to quantify how the long-time values of the populations approach the expected thermalized state as the bath approaches the thermodynamic limit. This approach should provide a good complement to state-of-the-art numerical methods, for which the long-time dynamics with large baths are impossible to simulate in this phase. Additionally, our numerics on finite baths reveal the possibility for unbounded exponential growth in the memory kernel, a phenomenon rooted in the appearance of exceptional points in the projected Liouvillian governing the reduced dynamics. In small systems amenable to exact numerics, we find that these pathologies may have some correlation with delocalization.

1. Introduction

Central spin models are ubiquitous in physical and chemical settings, from electrons with hyperfine coupling to nuclear spins inside quantum dots [1, 2, 3, 4], to nitrogen-vacancy centers in diamond [5, 6, 7]. Depending on the couplings in these systems, the central spin may have long-lived, slow decaying dynamics suitable for quantum information applications. The role of the bath in these cases is relegated to modeling decoherence, and has not traditionally been considered to be important. The bath is usually taken to be non-interacting, an assumption which has proven fruitful in the development of analytical [8, 9, 10, 11, 12, 13, 14] and numerical [15, 16, 17, 18, 19, 20] techniques. As such, these classes of baths—whether composed of bosons [21] or spins [22]—are by now reasonably well understood [22, 23, 24, 25, 26, 27, 28, 29, 30].

Recent research has brought new focus to modifications of the bath by adding, for example, intra-bath interactions and disorder. With these additions, the bath alone can exhibit novel dynamical phases such as many-body localization (MBL), which serves as a basis for nonergodicity in generic systems with strong disorder. Upon coupling to a bath, the long-ranged mediated interactions between constituents of the bath can push the bath towards delocalization. Recent work [31, 32] has shown that a single qubit coupled centrally to a 1D MBL spin chain can preserve localization provided that the magnitude of the central coupling decays fast enough with the size of the bath. But generally in these types of models, analytical and numerical approaches become scant due to the presence of interactions in the bath and to the star-like geometry of problem.

The added complexity has a drawback in that such systems quickly become intractable computationally, even for small bath sizes of $\sim O(30)$ degrees of freedom. This is due to the exponential increase of states in the Hilbert space that are involved in the dynamics. Moreover, large intra-bath interactions and disorder can radically change the timescales of the bath and invalidate perturbative approaches to bath dynamics. In this context, the case of MBL (in one dimension) is special in that it allows for a non-perturbative description in terms of 'l-bits' [33, 34, 35, 36]. Owing to this and to the slow growth of entanglement entropy [37, 38], dynamics in the localized phase of MBL systems are by now well explored numerically and analytically [39, 40, 41, 36, 42]; however, these approaches generally fail on the ergodic side of the transition.

The dynamics of extended, thermalizing many-body systems are typically very difficult to simulate exactly due to the rapid growth of entanglement. This is, for example, the limiting factor in methods based on a tensor network ansatz for the wavefunction in which the bond dimension bounds the amount of entanglement entropy that can be captured. A reasonable strategy then would be to extend the timescale of the converged simulation using information that can be computed on the timescales before the breakdown of the numerical method. Such an approach had been used successfully in the past to find the steady state behavior of quantum impurity systems [43, 44, 45], and to show the existence of bistability in the Anderson-Holstein model [46]. In those applications, the nontrivial dynamics of the impurity could be described exactly using a

memory kernel, derived using the projection operator formalism described by Nakajima, Zwanzig and Mori [47, 48, 49].

While the Nakajima-Zwanzig theory is formally exact, it is oftentimes more demanding than other formalisms to describe the dynamics because of the time-nonlocal memory kernel that naturally arises in their approach. It only becomes computationally useful if the nonlocality can be restricted, e.g. large timescale separation between bath and system dynamics lending to Markovian approximations, or if memory kernel decays sufficiently rapidly such that it can be truncated for times $\geq t_c$, where t_c is the cutoff time.

In this paper we study the memory kernel of a two-level system immersed in a bath modeled by a many-body localizable spin chain. We do so with two goals in mind: to assess the feasibility of extending the system dynamics from short time calculations when analytical and direct numerical approaches to compute the system dynamics fail (i.e. on the thermalizing side of the MBL transition); and to understand how interactions and disorder in the bath affect the memory kernel in properties such as timescales and tail behavior.

To this end, we will work with a previously studied model [31] of a qubit ($\hat{\tau}^{x,y,z}$) coupled to a disordered Heisenberg chain of L spins-1/2 ($\hat{\sigma}_i^{x,y,z}$):

$$\begin{aligned}\hat{H} &= \hat{H}_S + \hat{H}_B + \hat{V}, \\ \hat{H}_S &= \Omega \hat{\tau}^z \\ \hat{H}_B &= J \sum_{i=1}^L \frac{1}{4} \hat{\sigma}_i^z \hat{\sigma}_{i+1}^z + \frac{1}{2} (\hat{\sigma}_i^+ \hat{\sigma}_{i+1}^- + \text{h.c.}) + \sum_{i=1}^L \frac{h_i}{2} \hat{\sigma}_i^z \\ \hat{V} &= \frac{\gamma}{L} \sum_{i=1}^L \frac{1}{4} \hat{\sigma}_i^z \hat{\tau}^z + \frac{1}{2} (\hat{\sigma}_i^+ \hat{\tau}^- + \text{h.c.})\end{aligned}\tag{1}$$

where the $\hat{\tau}$ and $\hat{\sigma}$ are Pauli matrices. The bath Hamiltonian \hat{H}_B corresponds to the disordered, isotropic Heisenberg chain, where we take $J = 1$. The system-bath coupling terms \hat{V} are likewise given by the Heisenberg interaction, with magnitude scaling as γ/L to ensure that localization can occur for finite γ . We shall refer to γ as the strength of the central coupling. Finally, as was done by Ref. [31], the magnetic field is set to $\Omega = 0$. The random longitudinal fields h_i are drawn independently and uniformly from $[-W, W]$. In the high frequency limit where $\Omega \gg L$, the intrinsic dynamics of the central qubit will be so fast that its dynamics effectively decouples from that of the bath's. Localization in this limit is independent of the qubit, and is dictated by MBL physics. We focus on the other extreme, where the qubit has no intrinsic dynamics and is instead entirely dependent on the magnitude of the Overhauser field it experiences from the bath.

The structure of this paper is as follows: we shall first define the memory kernel for reduced dynamics and consider the role of disorder averaging; then we shall analyze the physics underlying the memory kernel at short, intermediate, and long times; and finally we shall discuss the potential for the memory to be used to augment short-time

experimental or numerical data.

1.1. The Nakajima-Zwanzig equation

We quickly review the basics of the projection operator approach to generalized quantum master equations. Any given Hamiltonian can be split into contributions \hat{H}_S acting only on the system, \hat{H}_B acting only on the bath, and \hat{V} coupling the two. We will use the term “bath” as a shorthand for the set of physical degrees of freedom surrounding the central qubit. In particular, we do not assert the character of the bath to be unchanged by coupling to the system. To each of the three aforementioned operators is associated a corresponding Liouvillian superoperator ($\mathbb{L}_S \cdot \equiv [\hat{H}_S, \cdot]$, $\mathbb{L}_B \cdot \equiv [\hat{H}_B, \cdot]$, $\mathbb{L}_V \cdot \equiv [\hat{V}, \cdot]$) generating dynamics for the density matrix

$$i \frac{d\hat{\rho}}{dt} = i \frac{d}{dt} e^{-i\mathbb{L}t} \hat{\rho}_0 = \mathbb{L}\hat{\rho}(t) \equiv (\mathbb{L}_S + \mathbb{L}_B + \mathbb{L}_V)\hat{\rho}(t). \quad (2)$$

Oftentimes one is interested only in the dynamics of the system, in which case the bath degrees of freedom can be projected out by tracing over the bath on both sides of the equation, where the bath trace is

$$\text{Tr}_B \hat{O} = \sum_{s,s'}^{\dim \mathcal{H}_S} \sum_b^{\dim \mathcal{H}_B} |s\rangle \langle s'| \langle s \otimes b | \hat{O} | s' \otimes b \rangle. \quad (3)$$

This is used to define the system reduced density matrix,

$$\hat{\rho}_S(t) = \text{Tr}_B \hat{\rho}(t). \quad (4)$$

We shall additionally assume that the initial state is factorized, i.e. $\hat{\rho}_0 = \hat{\rho}_{S,0} \otimes \hat{\rho}_B$. By taking the bath trace defined in (3) on both sides of (2) and using $\text{Tr}_B \mathbb{L}_B = 0$, we arrive at the exact expression

$$i \frac{d}{dt} \hat{\rho}_S(t) = \mathbb{L}_S \hat{\rho}_S(t) + \text{Tr}_B (\mathbb{L}_V e^{-i\mathbb{L}t} (\hat{\rho}_{S,0} \otimes \hat{\rho}_B)), \quad (5)$$

which is an equation of motion for $\hat{\rho}_S(t)$ that explicitly depends on knowledge of the time evolution of the full system and bath. This equation of motion can be closed, i.e. involving only $\hat{\rho}_S(t)$, by using Dyson’s identity (see [50, 51]):

$$i \frac{d}{dt} \hat{\rho}_S(t) = \mathbb{L}_S \hat{\rho}_S(t) - \int_0^t d\tau \mathbb{K}(t - \tau) \hat{\rho}_S(\tau). \quad (6)$$

The memory kernel superoperator is formally defined as

$$\mathbb{K}(t) \hat{\rho}_S = \text{Tr}_B (\mathbb{P} \mathbb{L} \mathbb{Q} e^{-i\mathbb{Q} \mathbb{L} \mathbb{Q} t} \mathbb{Q} \mathbb{L} \hat{\rho}_S \otimes \hat{\rho}_B). \quad (7)$$

In the above equation, the projection superoperator is taken to be $\mathbb{P} \cdot \equiv \text{Tr}_B(\cdot) \otimes \rho_B$ and $\mathbb{Q} = \mathbb{I} - \mathbb{P}$ is its complement. It is useful to define the system reduced propagator (superoperator) such that

$$\mathbb{U}_S(t) \hat{\rho}_{S,0} \equiv \hat{\rho}_S(t) = \text{Tr}_B (e^{-i\mathbb{L}t} \hat{\rho}_{S,0} \otimes \hat{\rho}_B). \quad (8)$$

Knowledge of \mathbb{U}_S allows for the generation of $\hat{\rho}_S(t)$, and lets us write a Nakajima-Zwanzig equation [52] involving only objects of one type, i.e. superoperators:

$$\frac{d}{dt} \mathbb{U}_S(t) = -i\mathbb{L}_S \mathbb{U}_S(t) - \int_0^t dt' \mathbb{K}(t - t') \mathbb{U}_S(t'), \quad (9)$$

In this form, it becomes clear that one can solve for \mathbb{K} directly from \mathbb{U}_S . Note that no approximations have been made and the dynamics generated by solving (9) and (7) are equivalent to solving (2) with the stated assumptions on initial conditions.

The derivation however, benefits from a simplification made possible by the form of the model Hamiltonian in (1). Bath traces over the interaction Liouvillian \mathbb{L}_V with respect to a bath state $\hat{\rho}_B$ of fixed magnetization will be zero due to the conservation of total magnetization in the model, and if we choose $\hat{\rho}_B$ to have zero magnetization. Therefore the validity of (7) is not restricted to solely thermal baths ($\hat{\rho}_B \propto e^{-\beta \hat{H}_B}$) nor bath eigenstates ($[\hat{\rho}_B, \hat{H}_B] = 0$).

The memory kernel \mathbb{K} and the system propagator \mathbb{U}_S , being linear mappings from the system Hilbert space \mathcal{H}_S to itself, can be represented as $(\dim \mathcal{H}_S)^2 \times (\dim \mathcal{H}_S)^2$ matrices. Requirements on unitarity and hermiticity, along with the decoupling of populations and coherences in this magnetization-conserving model, means that \mathbb{U}_S is described by only two independent entries when the focus is solely on population dynamics. The same extends to \mathbb{K} by virtue of its relation to \mathbb{U}_S . The two entries of \mathbb{U}_S are computed by two independent instances of the initial system state $\hat{\rho}_S(0)$: one from the population of the $|0\rangle$ state when $\hat{\rho}_S(0) = |0\rangle\langle 0|$, and the other from the population of the $|1\rangle$ state when $\hat{\rho}_S(0) = |1\rangle\langle 1|$. The initial bath state is the same in both cases, with definite magnetization $M_B = 0$. Because the total magnetization $\hat{M}^z = \hat{\tau}^z + \sum_i \hat{\sigma}_i^z$ is conserved, these two trajectories must reside in independent parts of Hilbert space. They are then combined in solving for the memory kernel, which can be done in the time domain by discretizing the integro-differential equation (see the supplementary materials for details). This, while posing no problem for the projection operator formalism, leads to a strange scenario where the central qubit dynamics restricted to one symmetry sector will depend on information from another, disjoint symmetry sector.

To skirt around this unsavory philosophical scenario, we can focus on only the population of the $|0\rangle$ state of the central qubit. Using the projection operator $\mathbb{P}\hat{\rho} = (|0\rangle\langle 0| \otimes \hat{\rho}_B) \text{Tr}[(|0\rangle\langle 0| \otimes \hat{I}_B)\hat{\rho}]$, one can repeat the same steps as before and obtain the scalar memory kernel for a single disorder realization as

$$K(t) = \text{Tr} \left[(|0\rangle\langle 0| \otimes \hat{I}_B) \mathbb{L} \mathbb{Q} e^{-i\mathbb{Q} \mathbb{L} \mathbb{Q} t} \mathbb{Q} \mathbb{L} (|0\rangle\langle 0| \otimes \hat{\rho}_B) \right], \quad (10)$$

satisfying the integro-differential equation

$$\frac{d}{dt} p_0(t) = - \int_0^t dt' K(t-t') p_0(t'), \quad (11)$$

or its Laplace-domain equivalent

$$\tilde{K}(z) = -z + \frac{1}{\tilde{p}_0(z)}. \quad (12)$$

Focusing on the population $p_0(t)$ of single state allows us to work with a scalar memory kernel $K(t)$ and simplifies the calculations. We will focus exclusively on the scalar memory kernel for the remainder of this paper. While this may be an unconventional choice of projector and therefore also of a memory kernel, we stress that the Nakajima-Zwanzig equation in its most general form does *not* depend on the choice of the \mathbb{P} . The

only requirement is that the same observables of interest are contained in the domains of the different projectors. ‡

Note that the memory kernel is akin to the self-energy for the reduced density matrix. Solving for it is then tantamount to solving the exact problem. Yet there are still advantages to working with the memory. For one, because of its relationship with the central qubit's populations it is in principle a measurable quantity. There is also the possibility for the memory to decay on timescales different from that of the populations. Should the memory decay much faster, then it may be possible to leverage the timescale separation to reduce the computational effort required to solve for the system dynamics at longer times.

1.2. Disorder averaged memory

Given that we are interested in disordered systems, suitable definitions of a memory kernel associated with different disorder realizations depends on the quantity of experimental interest. The difference depends on when the disorder averaging is performed. We denote by K_{avg} the case where the population p_0 is averaged over the disorder ($\overline{p_0}$) before solving for the memory kernel, satisfying

$$\frac{d}{dt}\overline{p_0}(t) = - \int_0^t dt' K_{\text{avg}}(t-t')\overline{p_0}(t'). \quad (13)$$

The other case, where the memory for disorder realization is found and then averaged, is denoted by \overline{K} . This latter case is relevant should one decide that the observable of interest is the memory kernel itself, which is in principle possible since it is directly computable from the populations.

It is not *a priori* clear how these two definitions are related. A reasonable guess might be that, upon disorder averaging, the two definitions are equivalent. We argue that this is not necessarily correct. Suppose that for every L the disorder-averaged population $\overline{p_0}(t)$ exists, with initial condition $\overline{p_0}(0) = 1$. The trajectory of the population for a single instance of disorder will have deviations from this average value, $p_0(t) = \overline{p_0}(t) + \delta p(t)$. Since populations must be positive at all times, so should their Laplace transforms for real, positive z . Using (12), the positivity of the Laplace transforms allows us to write

$$\begin{aligned} \widetilde{\delta K}(z) &= \frac{1}{\widetilde{\overline{p_0}}(z) + \widetilde{\delta p}(z)} - \frac{1}{\widetilde{\overline{p_0}}(z)} \\ &= \int_0^\infty du e^{-u(\widetilde{\overline{p_0}}(z) + \widetilde{\delta p}(z))} - e^{-u\widetilde{\overline{p_0}}(z)} \\ &= \int_0^\infty du e^{-u\widetilde{\overline{p_0}}(z)} \left(e^{-u\widetilde{\delta p}(z)} - 1 \right). \end{aligned} \quad (14)$$

Since the exponential function is entire, the term in parentheses can be expanded as a

‡ See [53] for a detailed demonstration of the equivalence of dynamics generated by different forms of generalized master equations resulting from the interplay of projections and the presence of conserved quantities.

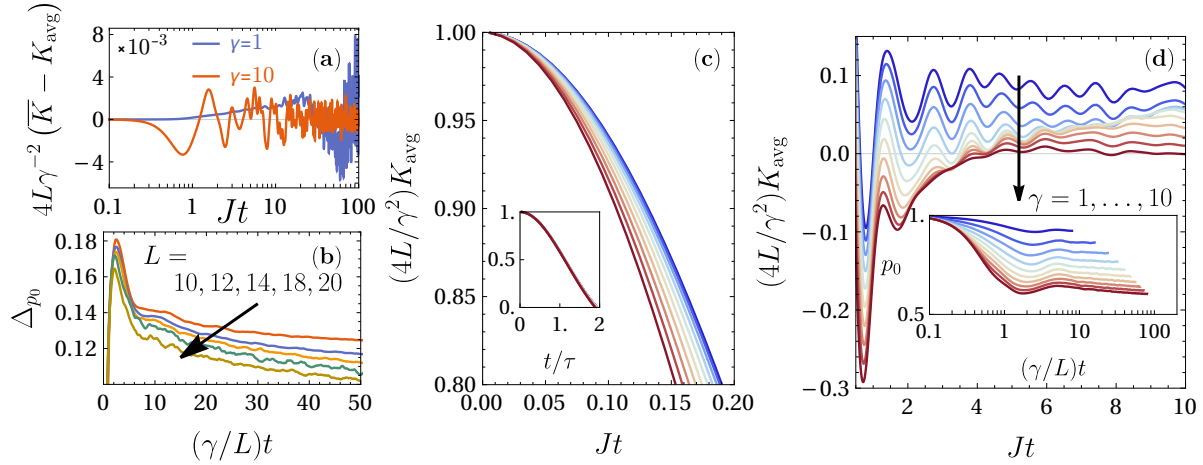


Figure 1. (a) Comparison of the averaged memory kernel \bar{K} and the memory kernel of the average K_{avg} for $L = 16$ deeply in the localizing ($\gamma = 1$) and thermalizing ($\gamma = 10$) phases, with ≥ 500 disorder realizations. (b) Root-mean-squared fluctuations Δ_{p_0} of the population for $\gamma = 10$. (c,d) The scalar memory kernel of the averaged population, $K_{\text{avg}}(t)$, for $L = 12$, onsite disorder strength $W = 6.0$, and with 6400 disorder realizations. The memory is rescaled such that its initial value is 1, and separated into the (c) short and (d) intermediate time regimes. For clarity, the data in the main panel of (d) are shifted up in multiples of 0.1 away from the $\gamma = 10$ curve. (c, inset) Collapse of the short time memory upon rescaling the time by τ defined in (17). (d, inset) The populations of the $|0\rangle$ state for the central qubit used to generate K_{avg} .

series,

$$\widetilde{\delta K}(z) = \int_0^\infty du e^{-u\widetilde{p_0}(z)} \sum_{n=1}^\infty \frac{(-u)^n}{n!} \left(\widetilde{\delta p}(z) \right)^n. \quad (15)$$

Averaging this expression over disorder, we will have the $n = 1$ term vanish by definition of δp . But all higher order terms—particularly ones with even powers—are not guaranteed to vanish. The consequence is that $K_{\text{avg}} \neq \bar{K}$ for finite L .

The situation is modified in the thermodynamic limit owing to self-averaging. Intuitively, a small subsystem interacting randomly with $N \gg 1$ degrees of freedom should have deviations from its mean behavior that decrease as N increases. As a result, when the environment is sufficiently large, a single realization of the random interaction should typically yield results close to the mean. This statement was recently demonstrated [54], showing that the system reduced density matrix enjoys the typicality property for system-bath interactions modeled by certain classes of random matrices. Importantly, [54] showed that this self-averaging property holds at least up to a timescale that increases with L . Note that to solve for $K(t)$ up to time T in (11) requires only $p_0(t)$ on $[0, T]$. Thus if $p_0(0 \leq t \leq T)$ is self-averaging, so must $K(t)$ on the same interval. In figure 1b we show the root-mean-squared fluctuations of $p_0(t)$ deeply in the thermalizing phase of the bath-disordered Hamiltonian (1), and observe that they indeed decrease with increasing bath size. Extrapolating to the

thermodynamic limit, we should therefore have self-averaging of the reduced density matrix of the central qubit. Then by extension the memory must self-average too. This can be seen from (15), where fluctuations of a single realization of $K(t)$ has deviations from $K_{\text{avg}}(t)$ that are bounded by the magnitude of the fluctuations in the population $\delta p(t) = p_0(t) - \overline{p_0}(t)$. In figure 1a, we find that $\overline{K}(t)$ and $K_{\text{avg}}(t)$ generally tend to differ by $|\overline{K}(t) - K_{\text{avg}}(t)| \sim O(10^{-3}(\gamma^2/4L))$ up to timescales $t \lesssim O(10^2)$ for the system sizes we can simulate. We observe that this deviation can diverge exponentially with a finite number of disorder realizations at long enough times, a phenomenon which we will return to in section 2.3. Barring that, the self-averageness of the population $p_0(t)$ —which yields $K_{\text{avg}}(t) = K(t) \implies K_{\text{avg}}(t) = \overline{K}(t)$ in the thermodynamic limit—gives us an alternate window into understanding how the memory kernel behaves. For the remainder of this paper, we shall mostly discuss $K_{\text{avg}}(t)$ as we are interested also in the dynamics of the averaged population.

2. Results

We implement time evolution by approximating $e^{-i\hat{H}t}$ with Chebyshev polynomials [55, 56]. To reduce computational costs, we use the conservation of total magnetization $\hat{M}^z = \hat{\tau}^z + \sum_i \hat{\sigma}_i^z$ in the model, allowing us to restrict the dynamics to the symmetry sector with $\hat{M}^z = -1$. The system is prepared in the $\hat{\rho}_{S,0} = |0\rangle\langle 0|$ state, while the bath state $\hat{\rho}_B$ is initialized to be a Neel state, $|\cdots \downarrow \uparrow \downarrow \uparrow \cdots\rangle$. We expect similar results should we choose different initial states within the sector of $\hat{M}^z = -1$.

A (matrix) memory kernel \mathbb{K} with n independent entries can be computed directly from the populations [52] using n different initial conditions, for each disorder realization. In this sense, there is added computational benefit to restricting our discussion to only the scalar memory kernel $K(t)$.

2.1. Short times

We can leverage the self-averaging property to gain some understanding of the short time behavior (figure 1c) of $K_{\text{avg}}(t)$. The derivatives of $K(t)$ at $t = 0$ for a single disorder realization can be found straightforwardly (see the supplementary materials) from those of $p_0(t)$, with the lowest orders being

$$\begin{aligned} K(t=0) &= -p_0^{(2)}(t=0) \\ K^{(2)}(t=0) &= -p_0^{(4)}(t=0) + \left(p_0^{(2)}(t=0)\right)^2, \end{aligned} \quad (16)$$

where $f^{(n)}$ denotes the n -th derivative. After averaging over disorder with an initial Neel state in the bath, we have

$$\begin{aligned} \frac{K_{\text{avg}}(t)}{\gamma^2/4L} &\approx 1 - \frac{1}{2} \left(\frac{t}{\tau_K}\right)^2 + O(t^4) \\ \frac{1}{\tau_K} &\equiv \sqrt{\frac{W^2}{3} + \frac{3J\gamma}{4L} + \frac{3\gamma^2}{4L} - \frac{3\gamma^2}{4L^2}}, \end{aligned} \quad (17)$$

where $J = 1$ in our model, and L is the number of spins in the bath. We see that the disorder strength W sets the initial decay rate $1/\tau_K$. This can be roughly estimated for large W from Fermi's Golden Rule, using our argument that disorder-averaging effectively gives us a continuous spectrum with an effective (root-mean-squared) bandwidth $\sim O(W\sqrt{L})$, and a coupling strength $\sim (\gamma/2L)^2$. While W sets the decay timescale for $K_{\text{avg}}(t)$, it is the quantity $\gamma^2/4L$ that sets the overall magnitude of $K_{\text{avg}}(t)$ and so dictates the timescale for $p_0(t)$. We expect so from the following scaling argument: Assume that the memory kernel converges to a limiting form in the thermodynamic limit as

$$\lim_{L \rightarrow \infty} \frac{K_{\text{avg}}(t)}{\gamma^2/4L} = k(t), \quad (18)$$

where $k(t)$ is independent of L and has a short time expansion given by (17). From the Nakajima-Zwanzig equation,

$$\frac{dp_0}{dt} \approx -\frac{\gamma^2}{4L} \int_0^t d\tau k(\tau) p_0(t - \tau), \quad (19)$$

we rescale the time to $t' = (\gamma^r/L^s)t$ and obtain

$$\frac{dp'_0}{dt'} = -\frac{\gamma^{2-2r}L^{2s-1}}{4} \int_0^{t'} d\tau' k\left(\frac{L^s\tau'}{\gamma^r}\right) p'_0(t' - \tau'), \quad (20)$$

where $p'_0(t') \equiv p_0(t'/(\gamma^r L^{-s}))$. We seek exponents $r > 0$ and $s > 0$ such that $p'_0(t')$ will vary on the timescale $\Delta t' \sim 1$. With the rescaled time, the $k(L^s\tau'/\gamma^r)$ appearing in (20) will have largely decayed by $\tau' \sim \gamma^r L^{-s}/(W/\sqrt{3})$, a timescale much faster than that of $p'_0(t')$. Hence we can approximate $p'_0(t' - \tau')$ in (20) as a constant, and estimate the strength of memory effects by integrating $k(L^s\tau'/\gamma^r)$ up to its decay time. This is roughly given by

$$\left(\frac{\gamma^{2-2r}L^{2s-1}}{4}\right) \left(\frac{\gamma^r/L^s}{W/\sqrt{3}}\right) = \frac{\sqrt{3}}{4} \frac{\gamma^{2-r}}{W} L^{s-1}. \quad (21)$$

We require $s = 1$ in order to have a converged p'_0 on the timescale of t' in the thermodynamic limit. Furthermore, $r = 1$ so that a trivial rescaling of the Hamiltonian $\hat{H} \rightarrow \alpha\hat{H}$ would not alter the strength of the memory term. Thus we argue that the dynamics of the central qubit should proceed on the timescale $\tau_{p_0} \sim L/\gamma$, consistent with our initial assumption that the population dynamics proceed much more slowly than does its associated memory kernel. We show this rescaling of time in figure 1b and in the inset of figure 1d, where the former shows the fluctuations of $p_0(t)$ between disorder realizations for different system sizes at fixed $\gamma = 10$, and the latter shows $p_0(t)$ for fixed $L = 12$ across γ . These figures show that the lowest moments of the populations align on the timescale $\tau_{p_0} \sim L/\gamma$. This result is also consistent with the result of [31] on the central qubit's autocorrelation function, $\int d\tau \langle \hat{\tau}^z(t + \tau) \rangle \langle \hat{\tau}^z(\tau) \rangle$, where it was observed that there is an accumulation of spectral weight near $\omega \sim \gamma/L$.

With a clear separation between τ_K and τ_{p_0} , one may wonder whether the central qubit can be described by an effective master equation. At least deep in the localized

phase, the bath is too slow to act as an effective reservoir for the central system. Correlation functions of the bath are argued [57, 58] to decay as a power law $t^{-\zeta}$ with $0 < \zeta < 1$, which makes memory effects crucial in dictating the behavior of $p_0(t)$ at long times. We will return to discuss the long time behavior of the memory kernel below in section 2.3.

2.2. Intermediate times

As seen in figure 1d, the memory past $Jt \gtrsim 1$ takes on different behaviors depending on the coupling strength, with increasingly damped oscillations as the combined system and bath transitions from localization to thermalization. The inset of figure 1d shows that this behavior is not observable when looking solely at the populations. The oscillation is dominated by frequencies in the range $\omega \in (4, 6)$, close to the disorder strength $W = 6$. Such oscillations are not a feature unique to an interacting bath. They show up in the non-interacting limit $J = 0$, in which the memory to lowest order in γ can be approximated by

$$K_{J=0}(t) \approx \frac{\gamma_{\perp}^2}{L} \frac{\sin(Wt)}{Wt} + O(\gamma^3), \quad (22)$$

where $\gamma_{\perp} = \gamma/2$. We see that oscillations are linked to the finite bandwidth W of frequencies in the bath [43], which arises from precession about the local field on each site, $(h_i/2)\hat{\sigma}_i^z$, and $h_i \in [-W, W]$. When interactions in the bath are turned on, we would expect them to provide a small renormalization to the precession frequencies, as we are working with a hierarchy of scales such that $W \gg J > \gamma$. This assumes, of course, that the bath dynamics are approximately describable with a precession picture even in the presence of bath interactions.

To justify this picture more formally, we can leverage the description of MBL systems in terms of quasi-local integrals of motion, which form the effective bath degrees of freedom that exhibit precession. At intermediate times and at weak coupling, the memory kernel can be approximated by bath correlation functions [59, 60],

$$K(t) \approx \frac{\gamma_{\perp}^2}{L^2} \sum_{i,j,\pm} \text{Tr} [\hat{\sigma}_i^{\pm}(t) \hat{\sigma}_j^{\mp}(0) \hat{\rho}_B]. \quad (23)$$

In the MBL phase, the bath spin operators $\hat{\sigma}_i^{\pm}$ have large overlaps [33] with quasi-local operators $\hat{\Theta}_i^{x,y,z}$ with which the bath Hamiltonian can be written as [33, 35, 58]

$$\hat{H}_B = \sum_{i=1}^L \varepsilon_i \hat{\Theta}_i^z + \sum_{i,j} J_{i,j} \hat{\Theta}_i^z \hat{\Theta}_j^z + \dots, \quad (24)$$

where the operators $\hat{\Theta}_i^{x,y,z}$ follow the Pauli commutation relations. The bath correlation functions oscillate according to ε_i , at least when the bath is strongly localized. The distribution of ε_i will therefore dictate the intermediate-time behavior of the memory kernel. For instance, if the distribution has sharp cutoffs like in the case of box disorder, then it can be expected that the memory will display oscillatory behavior whenever

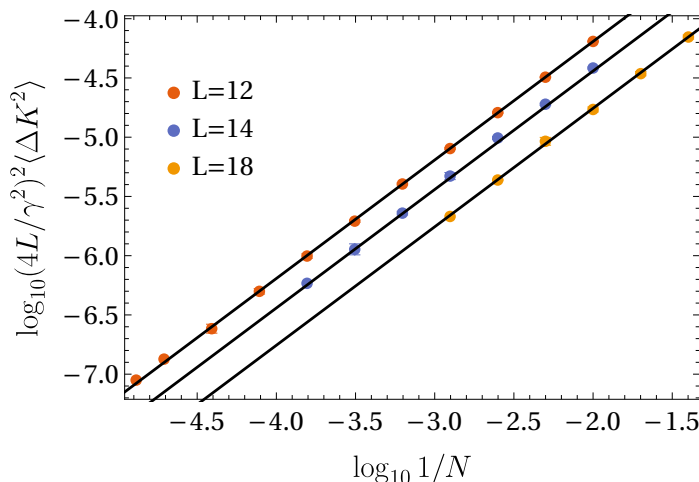


Figure 2. Average squared deviations on $t \in [50, 100]$ of $K_{\text{avg}}(t)$ in the thermalizing regime ($\gamma = 10$), as a function of disorder realizations N . Solid lines denote $1/N$ decay and serve as guides to the eye.

the stated approximations are applicable. We note that the picture of precessions is complicated at later times by dephasing mechanisms arising from interactions—the 2-body $J_{i,j}$ terms and higher—in the bath. Therefore, measurement of the memory kernel will yield some information on the parameters entering the bath Hamiltonian (24).

At the other extreme, where the system strongly couples ($\gamma \gtrsim 5$ for the value of $W = 6$ we have shown in figure 1d) to the bath, the localization assumed above breaks down [32]. That is, the bath interactions mediated by the qubit are strong enough that the bath cannot remain “close” to its initial state, so the expansion of the memory in terms of bath correlation functions no longer holds. In all, the contribution of the bath to the system dynamics can no longer be parsed into contributions from (nearly) independent oscillators. Instead, delocalization evidently serves to homogenize the influence of the bath, smoothing over the randomness from the local fields h_i , and damping out oscillations in $K_{\text{avg}}(t)$ as observed in the red curves of figure 1d.

2.3. Long times

Within the particular parameters we have chosen to study in this model, we define “long times” to correspond to $Jt \gtrsim 10$, a time past which the coherent oscillations in the bath have dephased. For the purpose of extrapolating the dynamics, it is crucial to understand how quickly $K_{\text{avg}}(t)$ decays, if it even does so at all. However, since we can only numerically average over a finite number N of disorder realizations, we cannot expect to observe a clear decay signal. Instead, we can ask whether the long time behavior of $K_{\text{avg}}(t)$ is consistent with small, possibly vanishing, values should we extrapolate our results to infinite N . Deeply in the thermalizing phase, we show in figure 2 that the magnitude of time-averaged fluctuations

$$\langle \Delta K^2 \rangle_{[T_i, T_f]} = \langle K_{\text{avg}}^2(t) \rangle_{[T_i, T_f]} - \langle K_{\text{avg}}(t) \rangle_{[T_i, T_f]}^2, \quad (25)$$

in the tail portion $K_{\text{avg}}(50 \leq t \leq 100)$ decays as $1/\sqrt{N}$, and moreover decreases with increasing system size as would be expected from self-averaging systems. In the above equation, we use the notation $\langle g(t) \rangle_{[T_i, T_f]} = \int_{T_i}^{T_f} dt g(t)/(T_f - T_i)$.

The persistence of the finite N noise makes it difficult to conclusively show numerically whether $K(t)$ decays as algebraically or exponentially. While in section 2.1 we argued for a power law decay for the weakly coupled, localized phase based on known phenomenology of MBL, this approach cannot work for the strongly coupled, thermalizing phase. In the absence of weak coupling perturbative expansions we now turn to the self-averaging relations $K_{\text{avg}} \sim K \sim \overline{K}$ to attempt to extract insights about the thermalizing phase. Doing so requires discussion about the memory kernel for a single realization of disorder, which is what we shall focus on for the remainder of this subsection.

For certain realizations of $\{h_i\}$, we observe an increasing likelihood for the memory—both scalar- and matrix-valued versions—to display unbounded exponential divergences with increasing coupling γ . We can verify the divergence for small system sizes $L \lesssim 6$, where the Laplace transformed memory kernel can be computed directly to yield the memory as a sum over simple poles, some of which with positive real parts. Such contributions—which are necessary in order to correctly reproduce the population dynamics—lead to an unbounded exponential *increase* of the memory for particular values of the coupling and magnitude of disordered fields. We will return to discuss the origins and implications of such pathological behavior in section 4.

We can motivate the consequences of exponentially growing contributions to $K(t)$ by examining the structure of the poles of its Laplace transform, $\tilde{K}(z)$. Because the Hamiltonian is real and Hermitian, poles of $\tilde{K}(z)$ are given by a real polynomial (see the supplementary materials for details). The polynomial will only involve terms of even powers, z^{2n} , because $p_0(t) = p_0(-t)$. Thus if a pole s_n exists with residue r_n such that $\text{Re } s_n \neq 0$, it must be the case that poles $-s_n$, s_n^* and $-s_n^*$ must exist with residues r_n , r_n^* , and r_n^* respectively. Based on the distribution of the pole structure, any exponentially dampened part of the memory ($\text{Re } s_n < 0$) must be accompanied by an exponentially growing counterpart. We posit that in the thermodynamic limit one of two situations must hold: 1) all off-axis poles converge towards the $\text{Im } z$ axis as $L \rightarrow \infty$, or 2) some poles still exist off-axis, which because of the conjugate pairs, contributes both exponential decay and growth. In the first scenario, there are no isolated poles to cause exponential decay. In the second scenario, any exponential decay is masked by exponential growth. Moreover, even if $\text{Re } s_n > 0$ poles cancel upon disorder averaging, the same would happen to the $\text{Re } s_n < 0$ poles by virtue of the relationship between residues discussed above. Therefore we argue that even in the thermalizing phase, the memory kernel for the dynamics we have defined should not exhibit exponential decay in the limit as $L \rightarrow \infty$. This leaves open the possibility of power-law or stretched-exponential behavior. In the next section, we will use infinite-time data from exact diagonalization to show that the long-time behavior of the memory is consistent with a power-law decay. Finally, we reiterate the importance of the order of limits in this

problem. They must be taken as

$$\lim_{t \rightarrow \infty} \lim_{L \rightarrow \infty} \lim_{N \rightarrow \infty} \quad (26)$$

to ensure that, reading from right to left, the population—and therefore the memory kernel—does not recur and to ensure the validity of the approximation $\bar{K} \approx K_{\text{avg}}$.

3. Extracting long time information from the memory kernel

The memory kernel has a direct relation to steady state values of the reduced density matrix, provided that a steady state exists [43, 44, 46, 45]. While the past work was done using all $d^2 \times d^2$ elements of the (matrix) memory kernel, we can import their ideas to the scalar memory kernel and a single element of the reduced density matrix. From the relationship between $\tilde{p}_0(z)$ and $\tilde{K}_{\text{avg}}(z)$, we can use the final value theorem to find

$$\begin{aligned} \lim_{z \rightarrow 0} z \tilde{p}_0(z) &= \lim_{z \rightarrow 0} \frac{1}{1 + \tilde{K}_{\text{avg}}(z)/z} \\ \lim_{t \rightarrow \infty} p_0(t) &= \lim_{z \rightarrow 0} \left[1 + \int_0^\infty dt e^{-zt} \overbrace{\int_0^t d\tau K_{\text{avg}}(\tau)}^{\equiv \kappa(t)} \right]^{-1}. \end{aligned} \quad (27)$$

If $\kappa(t)$ decays sufficiently quickly, we can extrapolate the $z \rightarrow 0$ limit from the finite times accessible from numerics. However, as we argued in the previous section, the memory cannot decay exponentially; therefore there is no single cutoff time t_c that can be used to approximate

$$\lim_{z \rightarrow 0} \int_0^\infty dt e^{-zt} \int_0^t d\tau K_{\text{avg}}(\tau) \approx \int_0^{t_c} dt \int_0^t d\tau K_{\text{avg}}(\tau). \quad (28)$$

A long time tail of $K_{\text{avg}}(t)$ would have non-negligible contributions to the dynamics, and therefore much care has to be taken in its use for extrapolations.

In lieu of a cutoff approximation, we turn again to the definition of K_{avg} ,

$$\tilde{K}_{\text{avg}}(z) = -z + \frac{1}{\tilde{p}_0(z)}. \quad (29)$$

We take an ansatz for the memory at small z ,

$$\tilde{\kappa}(z) \equiv \frac{\tilde{K}_{\text{avg}}(z)}{z} \approx \left(-1 + \frac{1}{p^\infty} \right) + a_0 z^\zeta + a_1 z, \quad (30)$$

where $0 < \zeta < 1$ and the long time limit of the average population $\bar{p}_0(t)$ shall be denoted as p^∞ . Note that we had argued in the previous section at least for the *absence* of exponential decay of the memory kernel in the thermodynamic limit, based on the structure of the poles in Laplace space. The presence of terms like z^ζ is consistent with long-time behavior as $\kappa(t) \sim t^{-\zeta-1} \implies K_{\text{avg}}(t) \sim t^{-\zeta-2}$.

To extrapolate the long time populations, we compute $\kappa(t)$ defined in (27) and approximate its Laplace transform

$$\tilde{\kappa}(z) \approx \int_0^{t_{\text{max}}} dt e^{-zt} \kappa(t). \quad (31)$$

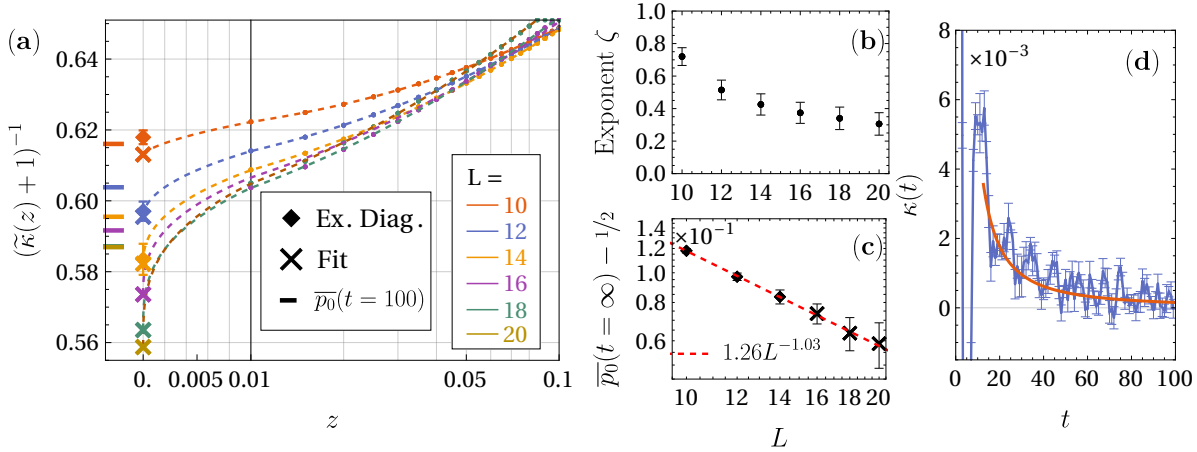


Figure 3. (a) Infinite time value of the average population \bar{p}_0 deeply in the thermalizing phase ($\gamma = 10$) using (27) and (30). Dashed lines and black crosses indicate respectively the fit to (30) and the extrapolated value for $t_c = \infty$. Where available, squares indicate the long time ($t \sim 10^{12}$) value of p_0 calculated independently from exact diagonalization. (b) Fitted exponents ζ as a function of system size. (c) Log-log plot of the long time limit of \bar{p}_0 versus the number of sites in the bath, L . Error bars in (b,c) of the extrapolated quantities ($L \geq 16$) correspond to 95% confidence intervals for the parameter estimation. (d) The integrated memory $\kappa(t)$ for $L = 12$ over 7.7×10^5 realizations of disorder. The red curve is the asymptotic time-domain behavior of $z^\zeta \Rightarrow t^{-1-\zeta}/\Gamma(-\zeta)$, as extracted from the fit to (30).

This result is then fitted using (30) to find p^∞ and b_0 and the amplitudes a_n . Such an approximation for the Laplace transform is admissible only if $\kappa(t)$ has decayed to sufficiently small values at $t = t_{\max}$, and for $z \gtrsim t_{\max}^{-1}$. We find that the results of using such an extrapolation procedure agree well with the values from independent calculations using exact diagonalization (figure 3a). Thus we are able to obtain estimates for the long-time population of the central qubit for system sizes ($L \gtrsim 16$) larger than those obtainable through exact diagonalization. In particular, this allows us to see how the central qubit approaches the thermalized limit $p_0 = 1/2$ with increasing bath size. In figure 3c, p^∞ is consistent with power law decay $p^\infty - 1/2 \sim L^{-1.03}$, which is in line with the scaling given by the infinite temperature phase space average,

$$\frac{\mathcal{H}_{|0\rangle}(M^z = -1)}{\mathcal{H}(M^z = -1)} = \frac{\binom{L}{L/2}}{\binom{L+1}{L/2}} = \frac{1}{2} + \frac{1}{2(L+1)}, \quad (32)$$

measuring the relative sizes of the Hilbert spaces for eigenstates occupying $|0\rangle$ and $|1\rangle$. We stress that because the memory must decay with time, this procedure cannot be used in finite systems for a single disorder realization, as the population will generally not reach a steady state in such circumstances.

Furthermore, since we have estimates of the true value of p^∞ obtained independently from exact diagonalization, we can compare (30) to a more generic alternative where $\tilde{\kappa}(z)$ is analytic about $z = 0$. Such is the case if $\kappa(t)$ were to, for example, decay exponentially or faster. For different system sizes and disorder distributions, we have

found that only the power-law ansatz is able to smoothly interpolate between known $z = 0$ values of $\tilde{\kappa}(z)$ from exact diagonalization and $z > 0$ values of $\tilde{\kappa}(z)$ calculated from finite time dynamics (see the supplementary materials for an example). Thus, while we have been unable to mathematically prove the existence of a long-tail in $K_{\text{avg}}(t)$, we have at least found numerical corroboration for the validity of our claim.

We note that, at least for $L \leq 14$, we find that the exponent ζ is system size dependent, for both box (figure 3b) and Gaussian distributed disorder. We further argue in the supplementary materials that if one takes the bath to initially be at infinite temperature, there will be a temporal power-law decay of the memory as $\sim t^{-3}$ which implies that $\zeta \rightarrow 1$ in this limit. Altogether, this suggests that ζ is at least a quantity dependent on the initial state; we cannot clarify whether there is a limiting value as $L \rightarrow \infty$ for initial states of fixed energy density, such as that considered in this work.

One may wonder what advantage this method confers to obtaining infinite-time populations, compared to simply simulating the population dynamics to longer time. For one, it is not always clear the timescales at which one can be sure that the system will have relaxed. This point is made more salient by the possibility of small, long-tailed memories which implies similar behaviors in the population dynamics. In this work, we have argued that it suffices to be able to observe whether the memory has reached the regime of power-law decay, at which point one can use (30). We stress that power-law behavior may become more apparent at earlier times in the memory than compared to the population, such as what we have observed in this work. While the $t^{-\zeta-1}$ contribution to $\kappa(t)$ may be subtle—on the order of 10^{-3} in all system sizes and disorder distributions we examined (see figure 3d for an example)—it is always possible to systematically improve its resolution simply by performing more disorder averaging.

4. Unbounded exponential growth of the memory kernel

We return now to the observation made in section 2.3 about memory kernels growing exponentially in time for certain realizations of the disorder. As seen in figure 4a, this can show up in the disorder averaged memory $\overline{K}(t)$, which can only be approximated via sampling over a finite number of disorder realizations. In figure 4b we show the maximum real part of the poles—corresponding to the maximum rate of exponential growth ν —for specific set of $\{h_i\}$ with $L = 4$. Intriguingly, ν is not monotonic with respect to γ , and displays square root singularities when going from $\nu = 0$ to finite ν . The sharpness of these singularities even with $L = 4$ indicates that they should not be associated with thermodynamic phase transitions. Instead, we believe they stem from exceptional points (EPs) in the generator of projected dynamics, $\mathbb{Q}\mathbb{L}\mathbb{Q}$, which are related to generalized avoided crossings. This generator is responsible for the time evolution of the memory kernel, as seen in (7). By choosing to focus on only a subset of all the physical degrees of freedom in the problem, we were forced to define projection operators \mathbb{P} that are not self-adjoint in the space of operators [61, 62]. For example, in operator space the projection operator associated with the scalar memory kernel is

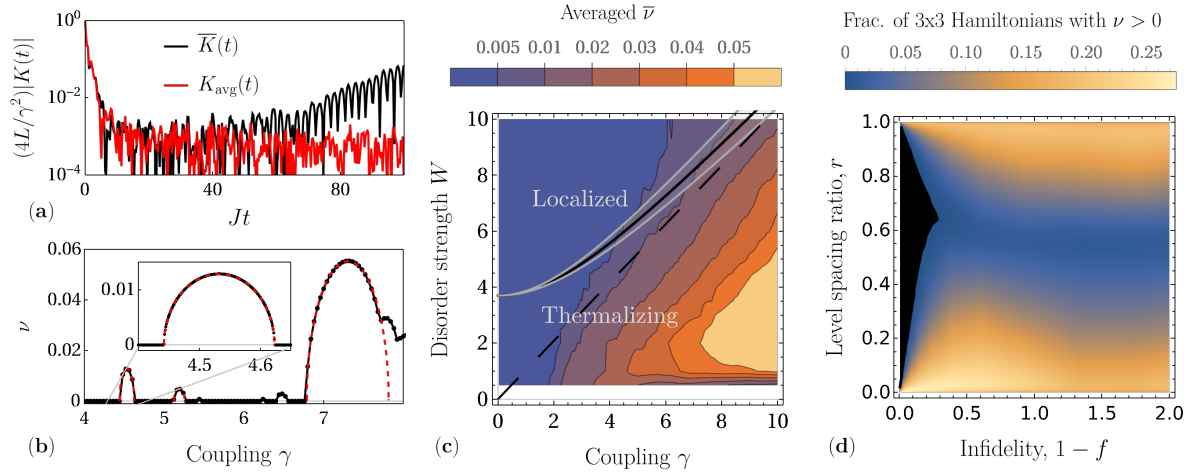


Figure 4. (a) The averaged memory kernel \bar{K} and the memory kernel of the averaged dynamics K_{avg} , for $L = 14$ and $\gamma = 10$. The two curves are approximately the same up to $t \lesssim 40$, past which they diverge exponentially owing to certain disorder realizations contributing to \bar{K} . (b) Maximum rate ν of exponential growth for $L = 4$ across a range of couplings with a fixed realization of disorder. The rate is computed by solving for the poles of Laplace-transformed memory kernel using 4096 bits of precision. Transitions from zero ν to finite ν are sharply discontinuous, and are well captured by fits to half ellipses (dashed red lines). (c) Disorder averaged $\bar{\nu}$ for $L = 4$. The black line and its surrounding error bands indicate the $L \rightarrow \infty$ phase boundary determined in Ref. [31]. The dashed black line is the asymptotic behavior of the boundary as argued in Ref. [32]. (d) Fraction of random real 3×3 Hamiltonians which show nonzero ν . The fidelity $f \in [-1, 1]$ quantifies the minimum overlap between the eigenstates with the system-bath decoupled basis, with $f = 1$ when they coincide (see main text and supplement for details). Black regions indicate a fraction of exactly zero within the 10^7 random configurations of eigenvectors sampled. The level spacing ratio is defined as $r \equiv \min(E_2 - E_1, E_3 - E_2) / \max(E_2 - E_1, E_3 - E_2)$ where $E_1 < E_2 < E_3$.

$\mathbb{P} = ||0\rangle\langle 0| \otimes \hat{\rho}_B)(|0\rangle\langle 0| \otimes \hat{I}_B|$, where the adjoint of the operator state vector has action

$$(\hat{A}|\hat{B}) = \text{Tr}(\hat{A}^\dagger \hat{B}). \quad (33)$$

The condition of being self-adjoint Liouville space is

$$\mathbb{P}^\dagger = \left(\sum_i |\hat{A}_i\rangle\langle \hat{B}_i| \right)^\dagger = \sum_i |\hat{B}_i\rangle\langle \hat{A}_i| = \mathbb{P}. \quad (34)$$

Writing \mathbb{P} in this way, it is clear that even if we project on to a thermal state of the bath, $\hat{\rho}_B \propto e^{-\beta H_B}$, the projector \mathbb{P} still cannot be self-adjoint unless the bath is in an infinite temperature state. Thus the projected Liouvillian QQLQ is also not self-adjoint, a property which allows EPs to occur. We have verified that the same phenomenon occurs even if we work with larger projection superoperators leading to matrix-valued memory kernels. We have additionally verified numerically that features unique to EPs such as the coalescence of eigenvalues and self-orthogonality are also present (see supplementary materials).

Interestingly, we note that the region in (W, γ) -space (figure 4c) for which MBL

is predicted to be stable in the thermodynamic limit appears to be correlated with a suppressed ν . While we are currently unable to prove that this is not a coincidence—such system sizes cannot inform us about the stability of MBL—it is possible that this provides a window into the character of the eigenstates, which are argued to be radically altered at large enough γ due to percolating networks of resonance states [32]. At the same time, it is known that the presence of exceptional points limits the radius of convergence for perturbative expansions [63, 64], and is postulated to be linked to quantum phase transitions [65, 66]. To fully explore any link between exceptional points, delocalization, and the breakdown of perturbative approaches to MBL will require a separate, in-depth study.

In the meantime, we can establish more indication of a connection between nonzero ν and localization in the following example in which an exponentially growing memory can occur. Consider a three-level system with nondenerate eigenvalues $0 = E_1 < E_2 < E_3$. Since the overall scale of the energies does not matter, we can condense these into one parameter given by the level spacing ratio

$$r = \frac{\min(E_2 - E_1, E_3 - E_2)}{\max(E_2 - E_1, E_3 - E_2)}. \quad (35)$$

By fixing the energies we can sample random real Hamiltonians by generating random orthogonal matrices, whose columns constitute the eigenstates. To make connection with the reduced dynamics we consider in this paper, we generate these eigenstates in the system-bath decoupled basis, $|0\rangle \otimes |B_{1\text{or}2}\rangle$ and $|1\rangle \otimes |B_3\rangle$. A linear combination of the basis states occupying $|0\rangle$ forms the initial state $\hat{\rho}(0)$. We quantify the relationship between the random eigenstates $|E_i\rangle$ and the decoupled basis $|SB_n\rangle$ through the fidelity,

$$F(E_1, E_2, E_3) = \min_{n=1,2,3} \max_{i=1,2,3} \langle E_i | SB_n \rangle, \quad (36)$$

and uniformly sample $|E_i\rangle$ to satisfy the constraint $F(E_1, E_2, E_3) \geq f$. The minimum fidelity f takes values between -1 and 1 . In figure 4d we show the maximum infidelity $1 - f$, which intuitively should play a similar role to the system bath coupling γ when both $1 - f$ and γ are small.

For each pair of (f, r) we can estimate the fraction of Hamiltonians and bath states—sampled uniformly subject to the constraint—that exhibit a nonzero ν . This result is shown in figure 4d. Exponential growth is seen to be prevalent near $r = 0$, which is when two eigenvalues of the Liouvillian become close to each other. This may be unsurprising given that exceptional points occur near level-crossings. More puzzling is the increasing prevalence of exponential growth as the level spacings become more uniform, i.e. as $r \rightarrow 1$. Finally, we observe zero instances of finite ν over 10^7 random samples of $|E_i\rangle$ inside a contiguous region beginning around $F \gtrsim 0.6$ (black region in figure 4d).

Heuristically speaking, delocalization with increasing coupling is the result of singular behavior in the full Hamiltonian, a fact which should be reflected in both the eigenstates and the spectrum. In finite systems, these may be isolated occurrences whose singular properties are smoothed out upon taking expectation values. Our numerical observations suggest that the non-Hermiticity of the projected Liouvillian is highly

sensitive to such singularities. We suspect this may be further indication of a deeper connection between localization and long-time pathologies in the memory kernel, but we are unable to clarify the underlying physics at this time. However, we will note that the situation may be altered by introducing a large bias on the central qubit, e.g. $\Omega\hat{\tau}^z$, the analysis of which we will leave for future work.

5. Discussion and conclusions

In this work we have undertaken the study of the time-nonlocal memory kernel describing how a many-body localizable “bath” affects the population dynamics of a central qubit. While the memory is formally defined in terms of Liouvillians, the dimensions of which quickly grow to be computationally intractable with increasing size of the Hilbert space, we are able to compute it numerically exactly from existing methods for simulating dynamics in closed quantum systems [52]. Thus we are able to directly examine the behavior of the memory kernel, parsing it into three regimes: short, intermediate, and long times.

On short timescales ($Jt \lesssim 1$) is where the majority of the memory’s decay occurs, irrespective of whether localization (at small γ) or delocalization (at large γ) is present. Properties of the memory on this timescale largely dictate the timescale of the dynamics for the central qubit’s populations. On intermediate timescales ($Jt \lesssim 10$) in the localized phase, the memory should exhibit dynamical signatures that result from the distribution of effective couplings for the emergent local integrals of motion describing the localized bath. For example, if the disorder distribution has sharp cutoffs, then this is manifest as oscillations in the memory. These oscillations are damped out as γ is increased, tuning the system and bath into the thermalized phase. Finally, at long times ($Jt \gtrsim 10$) we observe pathological exponential divergence of the memory kernel for certain realizations of disorder, deep in the thermalizing phase. We find that this comes from exceptional points in the projected Liouvillian generating the dynamics of the memory kernel, which come about at real values of the coupling γ due to the non-Hermiticity of the projection superoperator used to define the projected dynamics in the Nakajima-Zwanzig formalism. Unlike past work [61] that treated such exponential divergences as unphysical and should therefore be discarded, we have taken the view here that the divergences have a meaningful impact on the population dynamics. We argued that after disorder averaging the memory kernel, such pathological behaviors should preclude any exponential decay of the memory. Instead, we find that the tail of the memory is consistent with a power-law decay $\sim t^{-1-\zeta}$, where $0 < \zeta < 1$. Such an ansatz allows us to extract estimates of the disorder-averaged infinite-time population of the central qubit, solely from finite-time simulations. While such a procedure was shown in the past to work well when one could define a cutoff time for the memory kernel [43], here we have argued for the possibility that no cutoff time exists and demonstrated a proof-of-concept approach for extracting the infinite time populations in such a scenario.

In the model we have studied in this paper, we have taken the central coupling to

scale to zero as γ/L , in accordance with Refs. [32, 31] which have argued for its necessity to perturbatively preserve localized eigenstates. As a consequence, we have argued that there arises a separation of timescales between the population dynamics (τ_{p_0}) and its associated memory kernel (τ_K). Should we repeat our arguments from section 2.1 with a central coupling scaling as γ/L^q , we find that these two timescales remain separated for $q > 1/2$, but coincide for $0 < q \leq 1/2$. It is not clear whether such a separation of timescales—where $\tau_{p_0} \gg \tau_K$ as $L \rightarrow \infty$ —is required for the preservation of localization. Heuristically speaking however, having $\tau_{p_0} \gg \tau_K$ does not appear at first glance to be strong enough to preserve all aspects of MBL. One of the dynamical hallmarks of MBL is a logarithmically slow spreading of entanglement, i.e. spins on sites i and $i+L/2$ become entangled after a timescale $\sim \exp(L/2\xi)$ with ξ being the localization length [36]. Based on our view of the system dynamics from the memory kernel, the interaction between these two sites mediated by the central qubit should proceed on a timescales growing as a power of L , which is much shorter than the dephasing time $\sim \exp(L/2\xi)$ and thus may accelerate the dephasing process responsible for the slow dynamics in the MBL phase. However, it was noted in Ref. [31] that the central qubit at best facilitates a subextensive transport of magnetization which augments, but does not destroy, the logarithmic growth of bipartite entanglement.

Our work also raises tantalizing questions about possible connections between poles of the Laplace-transformed memory kernel and thermalization/delocalization. To this end, some work [63, 67, 68, 69] has been done to connect the proliferation of exceptional points in non-Hermitian systems to the appearance of quantum phase transitions and chaos. By focusing on a subpart of a closed system, we are forced to consider non-Hermitian *Liouvillians* giving rise to exceptional points in the space of operators. Explorations in this direction may benefit from insights from the physics of Feshbach resonances. Of course, we are severely limited by the system sizes amenable to numerical studies, thus we are able to do little more than remark on the coincidences we observe.

On the more practical side, we have demonstrated that there may be enough information from finite time dynamics to yield knowledge about long time limits, should they exist. While we have only demonstrated the extrapolation to $t = \infty$ of the population of the central qubit, we should in principle be able to use the same memory kernel and the Nakajima-Zwanzig equation in (10) to extend the computed dynamics to longer times. That this is even possible should not be too surprising, given that (10) when discretized over time gives the same form as the ansatz underlying linear prediction [70, 71], a method widely used for extending dynamical calculations. What we have shown in this work is that there may be more physical content in such a procedure than was previously appreciated. To explore these ideas more thoroughly warrants careful attention, particularly in regard to stability and applicability, which we shall leave for future work.

Finally, we note that any possibility of a pathological memory kernel at real γ can be erased by choosing to work with self-adjoint projection superoperators \mathbb{P} . One may be interested in doing so, for example, in order to approximate system dynamics from low

order, analytical expansions of the memory kernel. In that case it would be beneficial to know that the error introduced by the approximation is not exponentially divergent with time. It is as yet unclear whether self-adjoint projectors necessarily yield improvements, since pathological behaviors can still occur for complex couplings γ to limit convergence of naïve series expansions. We note, however, that previous work [72, 26] saw benefits from applying symmetry-adapted “correlated projectors”—which, we should point out, are manifestly self-adjoint in Liouville space—to low order expansions of the memory kernel. We leave clarification of this point for future work.

6. Acknowledgments

We are grateful to Amikam Levy, Sebastian Wenderoth, and Michael Thoss for useful discussions. This research used resources of the National Energy Research Scientific Computing Center, a U.S. Department of Energy Office of Science User Facility operated under Contract No. DE-AC02-05CH11231.

7. References

- [1] Schliemann J, Khaetskii A and Loss D 2003 *Journal of Physics: Condensed Matter* **15** R1809–R1833 URL <https://doi.org/10.1088/0953-8984/15/50/r01>
- [2] Witzel W M, Carroll M S, Morello A, Cywiński L and Das Sarma S 2010 *Phys. Rev. Lett.* **105**(18) 187602 URL <https://link.aps.org/doi/10.1103/PhysRevLett.105.187602>
- [3] Chekhovich E A, Makhonin M N, Tartakovskii A I, Yacoby A, Bluhm H, Nowack K C and Vandersypen L M K 2013 *Nature Materials* **12** 494–504 ISSN 1476-4660 URL <https://doi.org/10.1038/nmat3652>
- [4] Cogan D, Kenneth O, Lindner N H, Peniakov G, Hopfmann C, Dalacu D, Poole P J, Hawrylak P and Gershoni D 2018 *Phys. Rev. X* **8**(4) 041050 URL <https://link.aps.org/doi/10.1103/PhysRevX.8.041050>
- [5] Hanson R, Dobrovitski V V, Feiguin A E, Gywat O and Awschalom D D 2008 *Science* **320** 352–355 ISSN 0036-8075 (*Preprint* <https://science.sciencemag.org/content/320/5874/352.full.pdf>) URL <https://science.sciencemag.org/content/320/5874/352>
- [6] de Lange G, van der Sar T, Blok M, Wang Z H, Dobrovitski V and Hanson R 2012 *Scientific Reports* **2** 382 ISSN 2045-2322 URL <https://doi.org/10.1038/srep00382>
- [7] Bauch E, Singh S, Lee J, Hart C A, Schloss J M, Turner M J, Barry J F, Pham L M, Bar-Gill N, Yelin S F and Walsworth R L 2020 *Phys. Rev. B* **102**(13) 134210 URL <https://link.aps.org/doi/10.1103/PhysRevB.102.134210>
- [8] Dukelsky J, Pittel S and Sierra G 2004 *Rev. Mod. Phys.* **76**(3) 643–662 URL <https://link.aps.org/doi/10.1103/RevModPhys.76.643>
- [9] Claeys P W 2018 Richardson-gaudin models and broken integrability (*Preprint* [arXiv:1809.04447](https://arxiv.org/abs/1809.04447))
- [10] Villazon T, Chandran A and Claeys P W 2020 *Phys. Rev. Research* **2**(3) 032052 URL <https://link.aps.org/doi/10.1103/PhysRevResearch.2.032052>
- [11] Bortz M and Stolze J 2007 *Phys. Rev. B* **76**(1) 014304 URL <https://link.aps.org/doi/10.1103/PhysRevB.76.014304>
- [12] Bortz M, Eggert S, Schneider C, Stübner R and Stolze J 2010 *Phys. Rev. B* **82**(16) 161308 URL <https://link.aps.org/doi/10.1103/PhysRevB.82.161308>
- [13] Barnes E, Cywiński L and Das Sarma S 2012 *Phys. Rev. Lett.* **109**(14) 140403 URL <https://link.aps.org/doi/10.1103/PhysRevLett.109.140403>

- [14] Hall L T, Cole J H and Hollenberg L C L 2014 *Phys. Rev. B* **90**(7) 075201 URL <https://link.aps.org/doi/10.1103/PhysRevB.90.075201>
- [15] Wolf F A, McCulloch I P and Schollwöck U 2014 *Phys. Rev. B* **90**(23) 235131 URL <https://link.aps.org/doi/10.1103/PhysRevB.90.235131>
- [16] Wang H and Shao J 2012 *The Journal of Chemical Physics* **137** 22A504 (*Preprint* <https://doi.org/10.1063/1.4732808>) URL <https://doi.org/10.1063/1.4732808>
- [17] Diósi L and Strunz W T 1997 *Physics Letters A* **235** 569–573 ISSN 0375-9601 URL <https://www.sciencedirect.com/science/article/pii/S0375960197007172>
- [18] Orth P P, Imambekov A and Le Hur K 2013 *Phys. Rev. B* **87**(1) 014305 URL <https://link.aps.org/doi/10.1103/PhysRevB.87.014305>
- [19] Lindoy L P and Manolopoulos D E 2018 *Phys. Rev. Lett.* **120**(22) 220604 URL <https://link.aps.org/doi/10.1103/PhysRevLett.120.220604>
- [20] Faribault A and Schuricht D 2013 *Phys. Rev. B* **88**(8) 085323 URL <https://link.aps.org/doi/10.1103/PhysRevB.88.085323>
- [21] Leggett A J, Chakravarty S, Dorsey A T, Fisher M P A, Garg A and Zwerger W 1987 *Rev. Mod. Phys.* **59**(1) 1–85 URL <https://link.aps.org/doi/10.1103/RevModPhys.59.1>
- [22] Prokof'ev N V and Stamp P C E 2000 *Reports on Progress in Physics* **63** 669–726 URL <https://doi.org/10.1088/0034-4885/63/4/204>
- [23] Khaetskii A, Loss D and Glazman L 2003 *Phys. Rev. B* **67**(19) 195329 URL <https://link.aps.org/doi/10.1103/PhysRevB.67.195329>
- [24] Coish W A and Loss D 2004 *Phys. Rev. B* **70**(19) 195340 URL <https://link.aps.org/doi/10.1103/PhysRevB.70.195340>
- [25] Chen G, Bergman D L and Balents L 2007 *Phys. Rev. B* **76**(4) 045312 URL <https://link.aps.org/doi/10.1103/PhysRevB.76.045312>
- [26] Barnes E, Cywiński L and Das Sarma S 2011 *Phys. Rev. B* **84**(15) 155315 URL <https://link.aps.org/doi/10.1103/PhysRevB.84.155315>
- [27] Erbe B and Schliemann J 2012 *Phys. Rev. B* **85**(23) 235423 URL <https://link.aps.org/doi/10.1103/PhysRevB.85.235423>
- [28] Zhou X, Wan Q K and Wang X H 2020 *Entropy* **22** ISSN 1099-4300 URL <https://www.mdpi.com/1099-4300/22/1/23>
- [29] Nepomechie R I and Guan X W 2018 *Journal of Statistical Mechanics: Theory and Experiment* **2018** 103104 URL <https://doi.org/10.1088/1742-5468/aae2d9>
- [30] Jing J and Wu L A 2018 *Scientific Reports* **8** 1471 ISSN 2045-2322 URL <https://doi.org/10.1038/s41598-018-19977-9>
- [31] Hetterich D, Yao N Y, Serbyn M, Pollmann F and Trauzettel B 2018 *Phys. Rev. B* **98**(16) 161122 URL <https://link.aps.org/doi/10.1103/PhysRevB.98.161122>
- [32] Ponte P, Laumann C R, Huse D A and Chandran A 2017 *Phil. Trans. R. Soc. A.* **375** ISSN 1364-503X
- [33] Huse D A, Nandkishore R and Oganesyan V 2014 *Phys. Rev. B* **90**(17) 174202 URL <https://link.aps.org/doi/10.1103/PhysRevB.90.174202>
- [34] Nandkishore R and Huse D A 2015 *Annual Review of Condensed Matter Physics* **6** 15–38 (*Preprint* <https://doi.org/10.1146/annurev-conmatphys-031214-014726>) URL <https://doi.org/10.1146/annurev-conmatphys-031214-014726>
- [35] Imbrie J Z, Ros V and Scardicchio A 2017 *Annalen der Physik* **529** 1600278 (*Preprint* <https://onlinelibrary.wiley.com/doi/pdf/10.1002/andp.201600278>) URL <https://onlinelibrary.wiley.com/doi/abs/10.1002/andp.201600278>
- [36] Abanin D A, Altman E, Bloch I and Serbyn M 2019 *Rev. Mod. Phys.* **91**(2) 021001 URL <https://link.aps.org/doi/10.1103/RevModPhys.91.021001>
- [37] Žnidarič M, Prosen T c v and Prelovšek P 2008 *Phys. Rev. B* **77**(6) 064426 URL <https://link.aps.org/doi/10.1103/PhysRevB.77.064426>
- [38] Bardarson J H, Pollmann F and Moore J E 2012 *Phys. Rev. Lett.* **109**(1) 017202 URL <https://link.aps.org/doi/10.1103/PhysRevLett.109.017202>

- [//link.aps.org/doi/10.1103/PhysRevLett.109.017202](https://link.aps.org/doi/10.1103/PhysRevLett.109.017202)
- [39] Bar Lev Y, Cohen G and Reichman D R 2015 *Phys. Rev. Lett.* **114**(10) 100601 URL <https://link.aps.org/doi/10.1103/PhysRevLett.114.100601>
 - [40] De Tomasi G, Pollmann F and Heyl M 2019 *Phys. Rev. B* **99**(24) 241114 URL <https://link.aps.org/doi/10.1103/PhysRevB.99.241114>
 - [41] Alet F and Laflorencie N 2018 *Comptes Rendus Physique* **19** 498–525 ISSN 1631-0705 quantum simulation / Simulation quantique URL <https://www.sciencedirect.com/science/article/pii/S163107051830032X>
 - [42] Chanda T, Sierant P and Zakrzewski J 2020 *Phys. Rev. Research* **2**(3) 032045 URL <https://link.aps.org/doi/10.1103/PhysRevResearch.2.032045>
 - [43] Cohen G and Rabani E 2011 *Phys. Rev. B* **84**(7) 075150 URL <https://link.aps.org/doi/10.1103/PhysRevB.84.075150>
 - [44] Cohen G, Gull E, Reichman D R, Millis A J and Rabani E 2013 *Phys. Rev. B* **87**(19) 195108 URL <https://link.aps.org/doi/10.1103/PhysRevB.87.195108>
 - [45] Wilner E Y, Wang H, Thoss M and Rabani E 2014 *Phys. Rev. B* **89**(20) 205129 URL <https://link.aps.org/doi/10.1103/PhysRevB.89.205129>
 - [46] Wilner E Y, Wang H, Cohen G, Thoss M and Rabani E 2013 *Phys. Rev. B* **88**(4) 045137 URL <https://link.aps.org/doi/10.1103/PhysRevB.88.045137>
 - [47] Nakajima S 1958 *Progress of Theoretical Physics* **20** 948–959 ISSN 0033-068X URL <https://doi.org/10.1143/PTP.20.948>
 - [48] Zwanzig R 1960 *The Journal of Chemical Physics* **33** 1338–1341 URL <https://doi.org/10.1063/1.1731409>
 - [49] Mori H 1965 *Progress of Theoretical Physics* **33** 423–455 ISSN 0033-068X URL <https://doi.org/10.1143/PTP.33.423>
 - [50] Zwanzig R 1961 *Statistical Mechanics of Irreversibility* vol 3 (New York) p 106–141
 - [51] Singh N 2016 *Electronic Transport Theories* (CRC Press) URL <https://doi.org/10.1201/9781315368962>
 - [52] Kidon L, Wang H, Thoss M and Rabani E 2018 *The Journal of Chemical Physics* **149** 104105 (*Preprint* <https://doi.org/10.1063/1.5047446>) URL <https://doi.org/10.1063/1.5047446>
 - [53] Ng N, Limmer D T and Rabani E 2021 Note: Nonuniqueness of generalized quantum master equations for a single observable (*Preprint* [arXiv:2108.10937](https://arxiv.org/abs/2108.10937))
 - [54] Ithier G and Benaych-Georges F 2017 *Phys. Rev. A* **96**(1) 012108 URL <https://link.aps.org/doi/10.1103/PhysRevA.96.012108>
 - [55] Kosloff R 1994 *Annual Review of Physical Chemistry* **45** 145–178 (*Preprint* <https://doi.org/10.1146/annurev.pc.45.100194.001045>) URL <https://doi.org/10.1146/annurev.pc.45.100194.001045>
 - [56] Weiße A, Wellein G, Alvermann A and Fehske H 2006 *Rev. Mod. Phys.* **78**(1) 275–306 URL <https://link.aps.org/doi/10.1103/RevModPhys.78.275>
 - [57] Gopalakrishnan S, Müller M, Khemani V, Knap M, Demler E and Huse D A 2015 *Phys. Rev. B* **92**(10) 104202 URL <https://link.aps.org/doi/10.1103/PhysRevB.92.104202>
 - [58] Gopalakrishnan S and Parameswaran S 2020 *Physics Reports* **862** 1–62 ISSN 0370-1573 dynamics and transport at the threshold of many-body localization URL <https://www.sciencedirect.com/science/article/pii/S0370157320301083>
 - [59] Breuer H P, Petruccione F et al. 2002 *The theory of open quantum systems* (Oxford University Press)
 - [60] Nitzan A 2006 *Chemical Dynamics in Condensed Phases* (Oxford University Press) URL <https://doi.org/10.1093/oso/9780198529798.001.0001>
 - [61] Wilkie J 2001 *The Journal of Chemical Physics* **114** 7736–7745 URL <https://doi.org/10.1063/2F1.1365955>
 - [62] Wilkie J 2001 *The Journal of Chemical Physics* **115** 10335 URL <https://doi.org/10.1063/2F1.1365955>

- [63] Heiss W D 2012 Journal of Physics A: Mathematical and Theoretical **45** 444016 URL <https://doi.org/10.1088/1751-8113/45/44/444016>
- [64] Marie A, Burton H G A and Loos P F 2021 Journal of Physics: Condensed Matter URL <http://iopscience.iop.org/article/10.1088/1361-648X/abe795>
- [65] Jung C, Müller M and Rotter I 1999 Phys. Rev. E **60**(1) 114–131 URL <https://link.aps.org/doi/10.1103/PhysRevE.60.114>
- [66] Garmon S, Rotter I, Hatano N and Segal D 2012 International Journal of Theoretical Physics **51** 3536–3550 ISSN 1572-9575 URL <https://doi.org/10.1007/s10773-012-1240-5>
- [67] Heiss W D and Sannino A L 1990 Journal of Physics A: Mathematical and General **23** 1167–1178 URL <https://doi.org/10.1088/0305-4470/23/7/022>
- [68] Stránský P, Dvořák M and Cejnar P 2018 Phys. Rev. E **97**(1) 012112 URL <https://link.aps.org/doi/10.1103/PhysRevE.97.012112>
- [69] Cejnar P, Heinze S and Macek M 2007 Phys. Rev. Lett. **99**(10) 100601 URL <https://link.aps.org/doi/10.1103/PhysRevLett.99.100601>
- [70] Barthel T, Schollwöck U and White S R 2009 Phys. Rev. B **79**(24) 245101 URL <https://link.aps.org/doi/10.1103/PhysRevB.79.245101>
- [71] Schollwöck U 2011 Annals of Physics **326** 96–192 ISSN 0003-4916 january 2011 Special Issue URL <https://www.sciencedirect.com/science/article/pii/S0003491610001752>
- [72] Fischer J and Breuer H P 2007 Phys. Rev. A **76**(5) 052119 URL <https://link.aps.org/doi/10.1103/PhysRevA.76.052119>

Supplemental Material for “Signatures of a localizable bath in the memory kernel of a generalized quantum master equation”

Appendix A: Gaussian distributed disorder

In this section we show results for the same model, with h_i drawn iid from Gaussian distributions with the same mean and variance as that of the box model, $h_i \sim \mathcal{N}(0, \sigma^2 = W^2/3)$.

At weak couplings when there should be localization, we see in Fig. 1 that the distribution of disorder indeed has a strong effect on the memory in the intermediate time regime, as we argued in the main text.

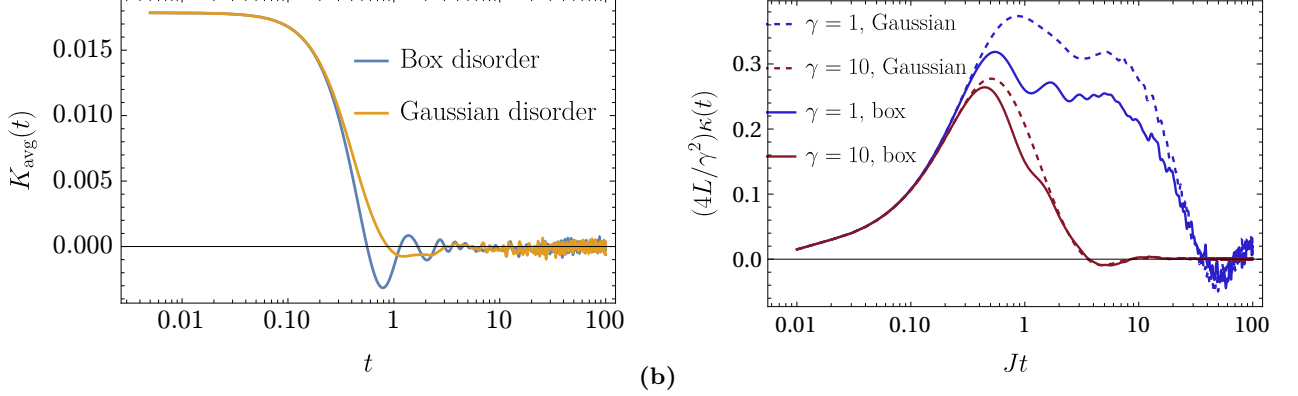


FIG. 1. **(a)** Memory kernel for the averaged population, $K_{\text{avg}}(t)$ for $L = 14$ at $\gamma = 1$. The intermediate time oscillations found in the case of box-distributed disorder are absent in the Gaussian-distributed case. **(b)** Integrated memory kernel for the averaged population, $K_{\text{avg}}(t)$ for $L = 14$ at $\gamma = 1$ (blue) and 10 (red), and for box (solid) and Gaussian (dashed) distributed disorder. The data shown is computed from 12800 realizations of disorder, except for the $\gamma = 1$ case with box disorder, which uses 1600 realizations.

The importance of the disorder distribution on intermediate timescales is clearly seen from the integrated memory, $\kappa(t) \equiv \int_0^t K_{\text{avg}}(\tau) d\tau$, in Fig. 1b. This figure shows also why extrapolation of the populations may be more feasible to attempt for the thermalizing phase as opposed to the localized phase, at least on the fixed simulation time $Jt_{\text{max}} = 100$.

The long-time behaviors of $K(t)$ are found to be qualitatively unchanged (see Fig. 2). There still exists exponential growth of the memory for certain realizations of disorder and the tail of $K_{\text{avg}}(t)$ is still consistent with a power-law decay, as seen through the application of the ansatz Eq. (29) of the main text.

Appendix B: Details on extrapolation of infinite-time populations

1. Long-time decay of memory with initially infinite temperature bath

We take the limit where the initial state has the bath at its infinite temperature state, i.e. $\hat{\rho}(0) = (|0\rangle\langle 0| \otimes \hat{I}_B)/\text{dim}\mathcal{H}_B$. In this case, the Laplace-transformed population is

$$\tilde{p}_0(z) = 2 \frac{1}{2(\text{dim}\mathcal{H}_B)} \sum_{E', E} \frac{\left| \langle E | |0\rangle\langle 0| \otimes \hat{I}_B | E' \rangle \right|^2}{z + i(E - E')},$$

which is exactly the Laplace transform of an infinite-temperature autocorrelation function

$$p_0(t - t') = 2C(t - t') \equiv 2 \text{Tr} \left\{ \frac{1}{2(\text{dim}\mathcal{H}_B)} \hat{p}_0(t) \hat{p}_0(t') \right\}.$$

We begin by assuming that the Hamiltonian is quantum chaotic at large couplings. After accounting for the symmetries present in the model, the spectrum of the Hamiltonian is assumed to follow the Wigner-Dyson distribution due to time-reversal invariance, and the eigenvectors appear like random vectors with respect to the product basis

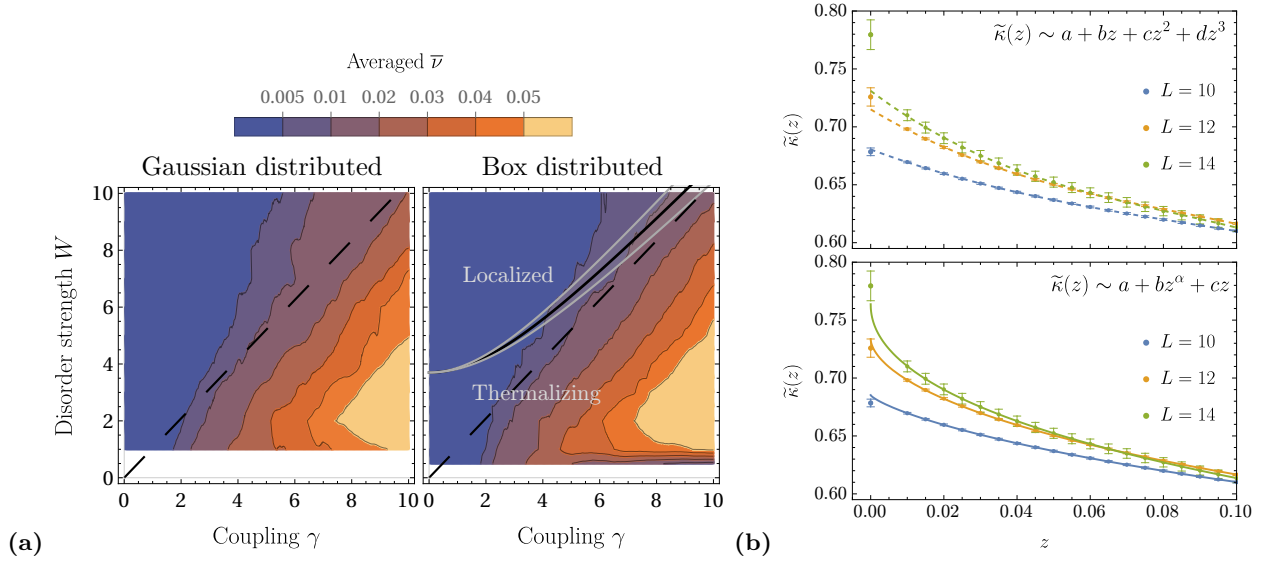


FIG. 2. Long-time behavior of the memory kernel for Gaussian distributed disorder. **(a)** Average rate of exponential growth for memory kernels in a single realization of disorder, where $L = 4$. The black dashed line in the Gaussian disorder case is the same as that for the box disorder, and is solely to help compare the two cases. **(b)** Extrapolation to $z = 0$ for the integrated memory kernel $\kappa(t)$, fitting to two ansatzes. Data points at $z = 0$ are independent calculations from exact diagonalization, while the data at $z > 0$ used for the fit are calculated using the Chebyshev polynomial method for time propagation.

$\{|0\rangle, |1\rangle\} \otimes \{|\uparrow\rangle, |\downarrow\rangle\}^L$. The small z limit of $\tilde{p}_0(z)$ is dominated by the statistics of small energy differences $E - E'$. This is because away from the edges of the energy spectrum, the matrix element of the local observable \hat{p}_0 should be constant in accordance with the random matrix assumption, i.e.

$$\left| \langle E | \hat{p}_0 | 0 \rangle \langle 0 | \otimes \hat{I}_B | E' \rangle \right|^2 \sim O\left(\frac{1}{4(\dim \mathcal{H}_B)}\right).$$

This assumption breaks down at large energy differences, so we expect that our calculation will only qualitatively reproduce the long-time behavior.

$$\begin{aligned} \tilde{p}_0(z) &\sim \frac{\text{constant}}{z} + \left(\frac{1}{2(\dim \mathcal{H}_B)}\right)^2 \sum_{E' \neq E} \frac{1}{z + i(E - E')} \\ &= \frac{\text{constant}}{z} + \frac{1}{2} \left(\frac{1}{2(\dim \mathcal{H}_B)}\right)^2 \sum_{E' \neq E} \frac{2z}{z^2 + (E - E')^2} \\ &= \frac{\text{constant}}{z} + \frac{1}{2} \left(\frac{1/\langle \Delta E \rangle}{2(\dim \mathcal{H}_B)}\right) \int d\omega \frac{2z}{z^2 + \omega^2} \underbrace{\sum_{E' \neq E} \left(\frac{1}{2(\dim \mathcal{H}_B)}\right) \delta\left[\frac{\omega - (E - E')}{\langle \Delta E \rangle}\right]}_{\equiv R_2(\omega/\langle \Delta E \rangle)}. \end{aligned}$$

Here, $R_2(\varepsilon)$ denotes the (unfolded) pair correlation function for the Gaussian orthogonal ensemble (GOE). The constant must equal $1/2$ by inspection, it being the final value of $p_0(t \rightarrow \infty)$. To estimate the small z behavior of $\tilde{p}_0(z)$, note that it will be largely determined by the behavior of $R_2(\omega/\langle \Delta E \rangle)$ for small ω . It is well known that the small ε behavior of $R_2(\varepsilon)$ is linear for GOE random matrices [78], from which we obtain the leading-order contribution to $\tilde{p}_0(z) \sim z \log z$. This translates to the time-domain as a t^{-2} decay. Thus we conclude that, if the Hamiltonian at strong couplings obeys random matrix theory, then the population dynamics with a bath at infinite temperature will relax as a power-law at long times.

2. Bias from finite realizations of disorder

One must take care in attempting to extrapolate to infinite times using only finite-time information on the memory kernel. As we argued in the main text, there appears a small contribution to $K(t)$ decaying much more slowly

compared to the transient behavior on timescales $Jt \lesssim 10$. At the same time, we note that the tail of $K(t)$ exhibits fluctuations between different samples of the disorder in the bath which, although decreasing in magnitude with increasing bath size, will still have nonnegligible influence on long-time extrapolations.

For N_s samples of the disorder, we can average these to obtain an estimate of the averaged population and its associated memory kernel,

$$p_0(t; N_s) = \frac{1}{N_s} \sum_{i=1}^{N_s} p_0^{(i)}(t)$$

$$\frac{d}{dt} p_0(t; N_s) = - \int_0^t d\tau K(t - \tau; N_s) p_0(\tau; N_s).$$

With these definitions, we therefore can identify

$$\begin{aligned} \overline{p_0}(t) &\equiv \lim_{N_s \rightarrow \infty} p_0(t; N_s) & K_{\text{avg}}(t) &\equiv \lim_{N_s \rightarrow \infty} K(t; N_s) \\ &\equiv \overline{p_0(t; N_s)}, \quad \forall N_s & &\neq \overline{K(t; N_s)} \quad (!) \end{aligned}$$

While the quantities on the right hands sides of the top lines are what we would like calculate, in practice we are only able to approximate the quantities in the bottom lines. Particularly, approximating $K_{\text{avg}}(t)$ using $\overline{K(t; N_s)}$ will introduce a bias that cannot be removed unless one takes the $N_s \rightarrow \infty$ limit. We can more formally analyze this approximation in Laplace space, where we have

$$\begin{aligned} \tilde{K}_{\text{avg}}(z) &= -z + \left(\overline{\tilde{p}_0(z; N_s)} \right)^{-1} \\ \overline{\tilde{K}(z; N_s)} &= -z + \left(\tilde{p}_0(z; N_s) \right)^{-1}. \end{aligned}$$

Note that the Laplace transform of $p_0(t; N_s)$ is positive for nonnegative z . Since $1/x$ is a convex function, these memory kernels can be related via Jensen's inequality,

$$\begin{aligned} \tilde{K}_{\text{avg}}(z) &\leq \overline{\tilde{K}(z; N_s)} \\ &\Downarrow \\ \frac{1}{1 + \tilde{K}_{\text{avg}}(z)/z} &\geq \frac{1}{1 + \overline{\tilde{K}(z; N_s)}/z}. \end{aligned}$$

Thus taking the $z \rightarrow 0^+$ limit, one sees that the extrapolated infinite-time populations may be underestimated if one uses $\overline{K(t; N_s)}$. The source of this systematic bias is due to the fact that $K(t)$ is a nonlinear function of $p_0(t)$. We would therefore like to estimate the magnitude of the nonlinearity to see if it will contribute significantly to the extrapolation of the infinite-time populations. If we formally consider $K(t)$ to be a function of $p_0(t)$ and expand around the infinitely-averaged result $\overline{p_0}(t)$, we have

$$K(t_n; N_s) = K(t_n; \infty) + \sum_m \left(p_0(t_m; N_s) - \overline{p_0(t_m)} \right) \partial_m K(t_n; \infty) \quad (\text{B1})$$

$$+ \frac{1}{2} \sum_{\ell m} \left(p_0(t_\ell; N_s) - \overline{p_0(t_\ell)} \right) \left(p_0(t_m; N_s) - \overline{p_0(t_m)} \right) \partial_\ell \partial_m K(t_n; \infty) + \dots \quad (\text{B2})$$

For a finite number of samples, αN_s where α is a positive integer, notice that the zeroth and linear order corrections can be cancelled

$$\begin{aligned} K(t_n; \alpha N_s) - \frac{1}{\alpha} \sum_{i=1}^{\alpha} K^{(i)}(t_n; N_s) &= \frac{1}{2} \sum_{\ell m} \left[\left(p_0(t_\ell; \alpha N_s) - \overline{p_0(t_\ell)} \right) \left(p_0(t_m; \alpha N_s) - \overline{p_0(t_m)} \right) \right. \\ &\quad \left. - \frac{1}{\alpha} \sum_{i=1}^{\alpha} \left(p_0^{(i)}(t_\ell; N_s) - \overline{p_0(t_\ell)} \right) \left(p_0^{(i)}(t_m; N_s) - \overline{p_0(t_m)} \right) \right] \partial_\ell \partial_m K(t_n; \infty) + \dots \\ &\equiv \delta K(t_n; \alpha N_s, N_s). \end{aligned}$$

We explicitly compare the magnitude of the relative correction $K(t_n; \alpha N_s, N_s)$ in Fig. 3.

We see that the relative bias is over an order of magnitude smaller compared to the fluctuations in $K(t)$ contributed by the finite number of disorder realizations, which appear as the linear-in- p_0 correction in Eq. (B1).

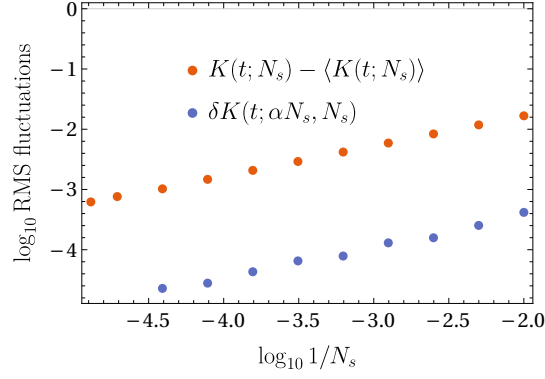


FIG. 3. Comparison between RMS fluctuations in the tail of $K(t)$ (orange dots) and RMS fluctuations in $K(t)$ resulting from bias introduced by a finite number of disorder realizations (blue dots). The system under consideration has $L = 12$ and $\gamma = 10$.

Appendix C: Numerical inversion for memory

Here we summarize the numerical method used to investigate the memory kernel without resorting to perturbation theory. For simplicity we shall restrict ourselves to the case of $H_S = 0$ with matrix memory kernels \mathbb{K} and system propagators \mathbb{U}_S :

$$\frac{d}{dt}\mathbb{U}_S(t) = - \int_0^t dt' \mathbb{K}(t')\mathbb{U}_S(t-t').$$

We assume that the value of $\mathbb{K}(0)$ is known, a fact which allows us to use slightly higher order approximations. For a general bath state ρ_B , the initial value is $\gamma_{\perp}^2 \sum_{i,j,\pm} \text{Tr} [\hat{\sigma}_i^{\pm} \hat{\sigma}_j^{\mp} \rho_B]$.

We discretize this equation as follows:

$$\begin{aligned} \dot{\mathbb{U}}_S(n\Delta t) &= \frac{1}{\Delta t} \left(\frac{-\mathbb{U}_S((n-1)\Delta t)}{3} + \frac{-\mathbb{U}_S(n\Delta t)}{2} + \mathbb{U}_S((n+1)\Delta t) + \frac{-\mathbb{U}_S((n+2)\Delta t)}{6} \right) + O(\Delta t^3) \\ \int_0^{n\Delta t} dt' \mathbb{K}(t')\mathbb{U}_S(n\Delta t - t') &= (\Delta t) \left(\frac{\mathbb{K}(0\Delta t)\mathbb{U}_S(n\Delta t) + \mathbb{K}(n\Delta t)\mathbb{U}_S(0\Delta t)}{2} + \sum_{m=1}^{n-1} \mathbb{K}(m\Delta t)\mathbb{U}_S((n-m)\Delta t) \right) + O(\Delta t^3). \end{aligned}$$

The calculations in the main paper were performed with $J\Delta t = 0.01$ for $0 \leq Jt \leq 100$. By truncating the error terms and equating the two expressions, the memory kernel can be solved for via iterating back substitutions. We note that the numerically inverted solution displays spurious oscillations of period $2\Delta t$. This can be largely removed by taking the 2-element moving average, i.e.

$$\mathbb{K} \left(\left(n + \frac{1}{2} \right) \Delta t \right) = \frac{\mathbb{K}(n\Delta t) + \mathbb{K}((n+1)\Delta t)}{2}.$$

For example, in the case of a scalar memory kernel generating the dynamics such that $K(t) = \exp(-t/5) \cos(t)$, such an averaging procedure produces a much more well-behaved solution (see Figure 4).

Appendix D: Scalar memory kernel

The derivation of the Nakajima-Zwanzig equation is agnostic with respect to choice of projection superoperators \mathbb{P} . Thus we have used this fact to our advantage in computing the memory kernel since projecting on to only a single distinguished variable, the $|0\rangle$ population,

$$\mathbb{P}_{\text{sca}} \hat{\rho} = (|0\rangle\langle 0| \otimes \hat{\rho}_B) \text{Tr} \left\{ (|0\rangle\langle 0| \otimes \hat{I}_B) \hat{\rho} \right\},$$

reduces the amount of independent trajectories required. This allows us to work with a scalar memory kernel, $K(t)$. We recognize that this is an unconventional choice of projector, with the usual choice being

$$\mathbb{P}_{\text{full}} \hat{\rho} = (\text{Tr}_B \hat{\rho}) \otimes \hat{\rho}_B,$$

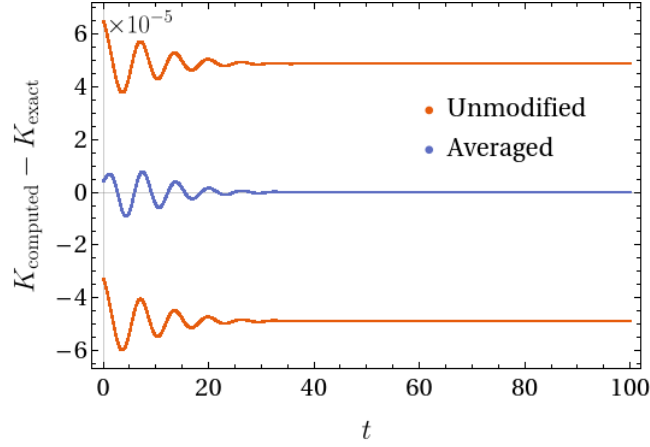


FIG. 4. Numerical inversion of dynamics generated by the memory kernel $K(t) = \exp(-t/5) \cos(t)$, compared against the exact solution. Without the 2-element moving average, the computed memory oscillates between the top and bottom bands on each timestep $\Delta t = 0.01$.

which gives rise to a tensor memory kernel $\mathbb{K}_{(mn),(ij)}$ describing how past values of the (ij) element of the system's reduced density matrix $\hat{\rho}_S$ affect the (mn) element of $\hat{\rho}_S$ at the current time.

The memory kernel in both cases follows the same form:

$$K(t) = \text{Tr} [\mathbb{P}_{\text{sca}} \mathbb{L} \mathbb{Q}_{\text{sca}} \exp \{-i \mathbb{Q}_{\text{sca}} \mathbb{L} \mathbb{Q}_{\text{sca}} t\} \mathbb{Q}_{\text{sca}} \mathbb{L} \mathbb{P}_{\text{sca}}] \quad (\text{D1})$$

$$\mathbb{K}(t) = \text{Tr} [\mathbb{P}_{\text{full}} \mathbb{L} \mathbb{Q}_{\text{full}} \exp \{-i \mathbb{Q}_{\text{full}} \mathbb{L} \mathbb{Q}_{\text{full}} t\} \mathbb{Q}_{\text{full}} \mathbb{L} \mathbb{P}_{\text{full}}]. \quad (\text{D2})$$

$$\dot{p}_0(t) = - \int_0^t d\tau K(t-\tau) p_0(\tau) \quad (\text{D3})$$

$$\dot{p}_0(t) = \int_0^t d\tau \mathbb{K}_{(11),(11)}(t-\tau) - \int_0^t d\tau [\mathbb{K}_{(00),(00)}(t-\tau) + \mathbb{K}_{(11),(11)}(t-\tau)] p_1(\tau). \quad (\text{D4})$$

The difference between these two expressions is that, in the former case where the scalar memory kernel is directly defined from a suitable projection operator, the state $|1\rangle$ in the central qubit is explicitly treated as part of the bath. In the second case where this was not done, the influence of the $|1\rangle$ state on the population of the $|0\rangle$ state manifests as an external fluctuating force, $\int_0^t \mathbb{K}_{(11),(11)}(\tau) d\tau$.

These two master equations can be shown to give the same dynamics since the memory kernels are related as,

$$K(t) = \int_0^t d\tau \mathbb{K}_{(00),(00)}(t-\tau) \dot{G}(\tau)$$

$$\dot{G}(t) = - \int_0^t d\tau \mathbb{K}_{(11),(11)}(t-\tau) G(\tau), \quad G(0) = 1.$$

Such a relation follows from the fact that the projection superoperators \mathbb{P}_{sca} and \mathbb{P}_{full} share a common term [76].

We can quickly derive the memory kernel in the eigenbasis by virtue of its relation with the trajectory $p_0(t)$. In the following, we adopt the notation: $|\psi_0\rangle$ denotes the initial bath state; $|0, B\rangle$ denotes the factorized state where the system is in $|0\rangle$ and the bath is in $|B\rangle$; and $|E\rangle$ denotes the eigenstate of energy E of the combined system and bath. The population, in the time and Laplace domains, is given by

$$p_0(t) = \sum_B \left| \sum_E e^{-iEt} \langle 0, B|E\rangle \langle E|0, \psi_0\rangle \right|^2$$

$$= \sum_B \sum_{E, E'} e^{-i(E-E')t} \langle 0, \psi_0|E'\rangle \langle E'|0, B\rangle \langle 0, B|E\rangle \langle E|0, \psi_0\rangle$$

$$\tilde{p}_0(z) = \sum_{E, E'} \underbrace{\left(\sum_B \langle E'|0, B\rangle \langle 0, B|E\rangle \right)}_{\equiv C(E', E)} \frac{\langle 0, \psi_0|E'\rangle \langle E|0, \psi_0\rangle}{z + i(E - E')}.$$

Since the memory kernel is defined as $K(z) = -z + p_0(z)^{-1}$, we therefore have, after using the fact that the inner products in the above expression are real,

$$K(z) = -z + \left(\sum_E \frac{C(E, E) |\langle E|0, \psi_0 \rangle|^2}{z} + 2z \sum_{E' > E} C(E', E) \frac{\langle 0, \psi_0 | E' \rangle \langle E | 0, \psi_0 \rangle}{z^2 + (E - E')^2} \right)^{-1}$$

Appendix E: Appearance of complex poles for the scalar memory kernel

To verify the exponential growth of $K(t)$ we observe from directly inverting the Nakajima-Zwanzig equation in the time domain, we solve for the poles of $\tilde{K}(z)$ numerically using 4096 bits of precision. Diagonalization and root-finding are respectively provided by the `GenericLinearAlgebra.jl` and the `PolynomialRoots.jl` packages in Julia. The rapid growth of the Liouville space's dimensionality limits this approach to system sizes $L \leq 6$.

The scalar memory kernel in Laplace space has a very simple form,

$$K(z) = -z + \left(\frac{\bar{p}_0}{z} + \sum_{n=1}^N \frac{A_n z}{z^2 + \omega_n^2} \right)^{-1},$$

where $\bar{p}_0 > 0$ is the value that $p_0(t)$ either decays to or oscillates around as $t \rightarrow \infty$. The frequencies ω_n are given by the difference of the n th pair of energies of the full Hamiltonian, $\omega_n = E' - E$ such that $E' > E$. The initial value of $p_0(0) = 1$ sets a constraint that $\bar{p}_0 + \sum_n A_n = 1$. The requirement that $0 \leq p_0 \leq 1$ gives the pair of sufficient conditions $\bar{p}_0 + \sum_n |A_n| \leq 1$ and $0 \leq \bar{p}_0 - \sum_n |A_n|$.

1. Exceptional points

For the Hamiltonian Eq. (1) of the main text, we illustrate our claim that there can exist exceptional points in the projected Liouvillian, which can then give rise to exponentially divergent scalar memory kernels. For simplicity, we fix $L = 2$ and take the bath to have zero magnetization. This makes the Hilbert space three-dimensional, and the Liouville space is therefore nine-dimensional. We can then directly write the Liouvillian $\mathbb{L} = [\hat{H}, \dots]$ and projector $\mathbb{P} = |\hat{\rho}(0)\rangle\langle 0| \otimes \hat{I}_B$ in matrix form, and compute the left and right eigendecompositions of $\mathbb{Q}\mathbb{L}\mathbb{Q}$. In Fig. 5a we show the (right) eigenvalue dynamics of $\mathbb{Q}\mathbb{L}\mathbb{Q}$ as the central coupling γ is tuned. The red dotted lines indicate the values of γ for which the projected Liouvillian becomes degenerate; the enumeration of all such exceptional points is shown in Fig. 5b. These are computed from the roots of the characteristic polynomial [?]]

$$\begin{aligned} g(\gamma) &= \det \mathbf{S}(\gamma) = 0 \\ \mathbf{S} &= \begin{pmatrix} \mu_{2N-2} & \mu_{2N-3} & \cdots & \mu_{N-1} \\ \mu_{2N-3} & \mu_{2N-4} & \cdots & \vdots \\ \vdots & \vdots & \mu_2 & \mu_1 \\ \mu_{N-1} & \cdots & \mu_1 & 1 \end{pmatrix} \\ \mu_p(\gamma) &= \sum_{i=1} (\hat{O}_i | \left(\mathbb{Q}\mathbb{L}(\gamma)\mathbb{Q} \right)^p | \hat{O}_i). \end{aligned} \tag{E1}$$

At one of these exceptional points, $\gamma = \gamma_c$ for example, it is evident from Fig. 5a that two eigenvalues have become exactly degenerate. In actuality, there is a *coalescence* of eigenvalues exactly at γ_c , which is when the left and right eigenvectors display self-orthogonality. This is explicitly demonstrated in Fig. 5c.

2. Three eigenvalues

The system of three states is simplest one for analyzing the exponential growth in the scalar memory kernel, since it yields only three unique positive energy differences. This in turn leads to a cubic equation $f_3(x)$ for the poles of the memory kernel, and the roots of cubic equations are well characterized by the sign of the discriminant. WLOG, we

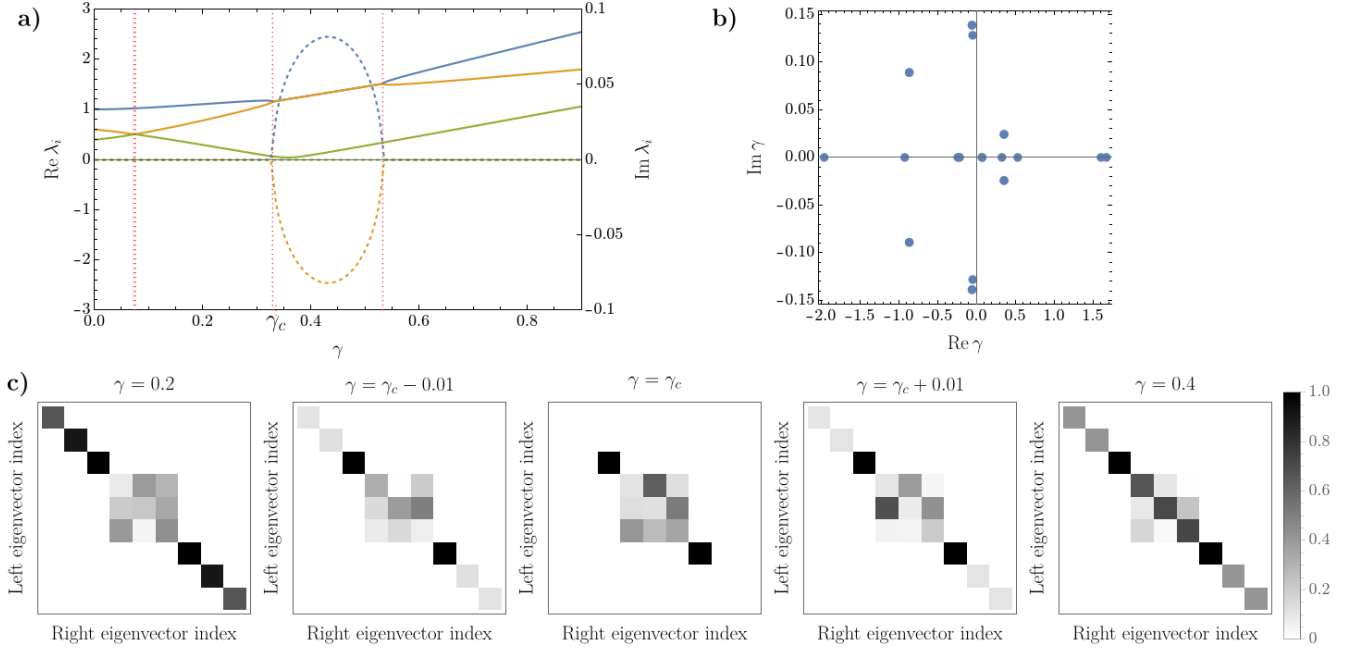


FIG. 5. Appearance of exceptional points in the projected Liouvillian $\mathbb{Q}\mathbb{L}\mathbb{Q}$ for the model studied in the main text with a fixed disorder configuration and $L = 2$. **(a)** Right eigenvalues of $\mathbb{Q}\mathbb{L}\mathbb{Q}$ as the central coupling γ is increased. When γ lies between two exceptional points on the branch singularity that connects them, the projected Liouvillian attains imaginary eigenvalues. **(b)** Exceptional points of $\mathbb{Q}\mathbb{L}(\gamma)\mathbb{Q}$ as obtained from Eq. (E1). **(c)** Squared overlaps of the left and right eigenvectors of the projected Liouvillian. Exactly at the exceptional point labelled γ_c , it is seen that there are left and right eigenvectors that become orthogonal.

define $\omega_1 = \Omega$, $\omega_2 = \delta$, and $\omega_3 = \Omega + \delta$, and the ratio of adjacent energy differences $r \equiv \delta/\Omega$. Since the physics should be invariant with respect to swapping Ω and δ , we shall limit our discussion of r on the restricted domain $[0, 1]$.

$$\begin{aligned}
 f_3(z^2) &= (z^2)^3 + \underbrace{((1 - A_1)\omega_1^2 + (1 - A_2)\omega_2^2 + (1 - A_3)\omega_3^2)}_{\equiv b} (z^2)^2 \\
 &+ \underbrace{((\bar{p}_0 + A_1)\omega_2^2\omega_3^2 + (\bar{p}_0 + A_2)\omega_1^2\omega_3^2 + (\bar{p}_0 + A_3)\omega_1^2\omega_2^2)}_{\equiv c} (z^2)^1 \\
 &+ \underbrace{\bar{p}_0\omega_1^2\omega_2^2\omega_3^2}_{\equiv d}
 \end{aligned}$$

This is a real cubic polynomial in the variable $x \equiv z^2$. The properties of its zeroes are communicated through the sign of its discriminant Δ , which for a general cubic equation $ax^3 + bx^2 + cx + d$ is given by

$$\Delta = b^2c^2 - 4ac^3 - 4b^3d - 27a^2d^2 + 18abcd.$$

When this quantity is negative, the equation will have two complex roots. Similarly, if $\Delta > 0$ and the coefficients of f_3 are strictly positive, there must be three real, negative roots. Assuming that $\bar{p}_0 > 0$ implies $d > 0$. We can therefore work with a modified discriminant by dividing through by d^2 , while retaining the properties of the original discriminant. Doing so results in

$$\begin{aligned}
 \Delta' &= \beta^2\gamma^2 + 18\beta\gamma - 4\gamma^3 - 4\beta^3 - 27 \\
 \beta &= b/d^{1/3} \\
 \gamma &= \gamma/d^{2/3}
 \end{aligned}$$

In terms of the ratio r , we have

$$\beta = \frac{1}{\overline{p_0}^{1/3}} \left((1 - A_1)r^{-2/3}(1+r)^{-2/3} + (1 - A_2)r^{4/3}(1+r)^{-2/3} + (1 - A_3)r^{-2/3}(1+r)^{4/3} \right)$$

$$\gamma = \frac{1}{\overline{p_0}^{2/3}} \left((\overline{p_0} + A_1)r^{2/3}(1+r)^{2/3} + (\overline{p_0} + A_2)r^{-4/3}(1+r)^{2/3} + (\overline{p_0} + A_3)r^{2/3}(1+r)^{-4/3} \right)$$

We find that the sufficient conditions provided by the bounds $0 \leq p_0 \leq 1 \implies \overline{p_0} + \sum_n |A_n| \leq 1$ and $0 \leq \overline{p_0} - \sum_n |A_n|$ is too strict and evidently produces no complex poles. Instead, we shall randomly sample the A_n 's and $\overline{p_0}$.

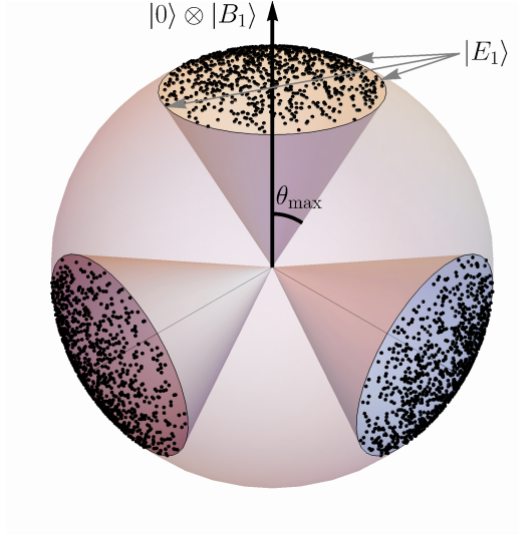


FIG. 6. Relationship between the system-bath decoupled basis (unit vectors on the x, y, z axes) and the randomly sampled eigenvectors (black dots). The parameter θ_{\max} controls the maximum deviation of the eigenvectors from the basis (shaded regions bounded by cones).

In this three-state case, we parametrize the eigenstates using the axis-angle representation, where for the k th eigenstate ($k = 1, 2, 3$),

$$\left(\mathbf{v}^{(k)} \right)_j = \left(e^{-i\theta(\hat{\mathbf{S}} \cdot \mathbf{n})} \right)_{j,k},$$

where the unit vector \mathbf{n} is defined by the polar angle ψ and the azimuthal angle ϕ . In terms of these three parameters, we define probability distribution as

$$P(\phi, \psi, \theta) d\phi d\psi d\theta = \frac{\sin \psi}{4\pi} \frac{1 - \cos \theta}{\theta_{\max} - \sin \theta_{\max}} d\phi d\psi d\theta,$$

on the domain $0 \leq \phi < 2\pi$, $0 \leq \psi \leq \pi$, and $0 \leq \theta \leq \theta_{\max}$, where $0 \leq \theta_{\max} \leq \pi$. As seen in Fig. 6, the angle θ_{\max} measures the maximum deviation between the eigenvectors and the system=bath decoupled basis states. This measure coincides with the Haar measure for the 3×3 circular orthogonal ensemble When $\theta_{\max} = \pi$. In the main text, we measure this deviation in terms of the minimum fidelity

$$f \equiv \cos \theta_{\max}.$$

Appendix F: Short time behavior of the memory kernel

In this section we reproduce the calculation for the short time behavior of the scalar memory kernel $K(t)$. The zeroth and second derivatives of $K(t)$ at $t = 0$ are given respectively by

$$K(t=0) = -p_0^{(2)}(t=0) \tag{F1}$$

$$K^{(2)}(t=0) = -p_0^{(4)}(t=0) + \left(p_0^{(2)}(t=0) \right)^2. \tag{F2}$$

For a single realization of disorder, we therefore need

$$\begin{aligned} p_0^{(2)}(t=0) &= -\text{Tr} \left((|0\rangle\langle 0| \otimes \hat{I}_B) [H, [H, |0\rangle\langle 0| \otimes \rho_B]] \right) \\ p_0^{(4)}(t=0) &= \text{Tr} \left((|0\rangle\langle 0| \otimes \hat{I}_B) [H, [H, [H, [H, |0\rangle\langle 0| \otimes \rho_B]]]] \right). \end{aligned}$$

Throughout the calculation we shall rely on the Pauli algebra,

$$[\hat{\sigma}^z, \hat{\sigma}^\pm] = \pm 2\hat{\sigma}^\pm \quad [\hat{\sigma}^+, \hat{\sigma}^-] = \hat{\sigma}^z \quad \{\hat{\sigma}^z, \hat{\sigma}^\pm\} = 0 \quad \{\hat{\sigma}^+, \hat{\sigma}^-\} = \hat{I},$$

along with the commutator identity for operators A_i that commute with B_i but not within each group,

$$[A_1 B_1, A_2 B_2] = [A_1, A_2] B_1 B_2 + A_2 A_1 [B_1, B_2] \quad (\text{F3})$$

$$= [A_1, A_2] \frac{\{B_1, B_2\}}{2} + \frac{\{A_2, A_1\}}{2} [B_1, B_2]. \quad (\text{F4})$$

We shall also make use of the following identity to reduce the number of nested commutators:

$$\text{Tr} (A [B, C]) = -\text{Tr} ([B, A] C).$$

In the following we shall assume that $[\sum_i \hat{\sigma}_i^z, \rho_B] = [\sum_i \hat{\sigma}_i^z, H_B] = 0$. The first commutators can be reduced to

$$\begin{aligned} [H, |0\rangle\langle 0| \otimes \hat{I}_B] &= [H_S, |0\rangle\langle 0| \otimes \hat{I}_B] + [H_B, |0\rangle\langle 0| \otimes \hat{I}_B] + [V, |0\rangle\langle 0| \otimes \hat{I}_B] \\ &= \gamma_\perp \sum_{i=1}^L \sum_{\pm} [\hat{\tau}^\pm \hat{\sigma}_i^\mp, |0\rangle\langle 0| \otimes \hat{I}_B] + \gamma_z \sum_{i=1}^L [\hat{\tau}^z \hat{\sigma}_i^z, |0\rangle\langle 0| \otimes \hat{I}_B] \\ &= \gamma_\perp \sum_{i=1}^L [1\rangle\langle 0| \otimes \hat{\sigma}_i^- - |0\rangle\langle 1| \otimes \hat{\sigma}_i^+] \\ [H, |0\rangle\langle 0| \otimes \hat{\rho}_B] &= [H_S, |0\rangle\langle 0| \otimes \hat{\rho}_B] + [H_B, |0\rangle\langle 0| \otimes \hat{\rho}_B] + [V, |0\rangle\langle 0| \otimes \hat{\rho}_B] \\ &= |0\rangle\langle 0| \otimes [H_B, \hat{\rho}_B] + \gamma_\perp \sum_{i=1}^L \sum_{\pm} [\hat{\tau}^\pm \hat{\sigma}_i^\mp, |0\rangle\langle 0| \otimes \hat{\rho}_B] + \gamma_z \left[\hat{\tau}^z \otimes \left(\sum_{i=1}^L \hat{\sigma}_i^z \right), |0\rangle\langle 0| \otimes \hat{\rho}_B \right] \\ &= |0\rangle\langle 0| \otimes [H_B, \hat{\rho}_B] + \gamma_\perp \sum_{i=1}^L [1\rangle\langle 0| \otimes (\hat{\sigma}_i^- \hat{\rho}_B) - |0\rangle\langle 1| \otimes (\hat{\rho}_B \hat{\sigma}_i^+)]. \end{aligned}$$

These two expressions allow us to immediately evaluate $p_0^{(2)}(t=0)$, giving

$$\begin{aligned} -p_0^{(2)}(t=0) &= \gamma_\perp \text{Tr} \left\{ \left(\sum_{j=1}^L |0\rangle\langle 1| \otimes \hat{\sigma}_j^+ - |1\rangle\langle 0| \otimes \hat{\sigma}_j^- \right) \left(|0\rangle\langle 0| \otimes [H_B, \hat{\rho}_B] + \gamma_\perp \sum_{i=1}^L [1\rangle\langle 0| \otimes (\hat{\sigma}_i^- \hat{\rho}_B) - |0\rangle\langle 1| \otimes (\hat{\rho}_B \hat{\sigma}_i^+) \right) \right\} \\ &= \gamma_\perp^2 \sum_{i,j=1}^L \text{Tr} \{ (|0\rangle\langle 1| \otimes \hat{\sigma}_j^+ - |1\rangle\langle 0| \otimes \hat{\sigma}_j^-) (|1\rangle\langle 0| \otimes (\hat{\sigma}_i^- \hat{\rho}_B) - |0\rangle\langle 1| \otimes (\hat{\rho}_B \hat{\sigma}_i^+)) \} \\ &= \gamma_\perp^2 \sum_{i,j=1}^L \text{Tr} (|0\rangle\langle 0| \otimes (\hat{\sigma}_j^+ \hat{\sigma}_i^- \hat{\rho}_B) + |1\rangle\langle 1| \otimes (\hat{\rho}_B \hat{\sigma}_i^+ \hat{\sigma}_j^-)) \\ &= \gamma_\perp^2 \sum_{i,j=1}^L \text{Tr}_B (\{\hat{\sigma}_j^+, \hat{\sigma}_i^-\} \hat{\rho}_B) = \gamma_\perp^2 \sum_{i,j=1}^L \text{Tr}_B (\{\hat{\sigma}_j^+, \hat{\sigma}_i^-\} \hat{\rho}_B) \\ &= L\gamma_\perp^2 + \gamma_\perp^2 \sum_{i \neq j}^L \text{Tr}_B (\{\hat{\sigma}_j^+, \hat{\sigma}_i^-\} \hat{\rho}_B). \end{aligned}$$

When the initial bath state has a single pattern of magnetization (i.e. it is a product state of $\hat{\sigma}_i^z$ eigenstates), the initial value of the memory kernel will be $K(t=0) = L\gamma_\perp^2$, independent of the disorder realization as well as intrabath interactions. The fact that $K^{(2)}(t=0)$ is linear in the disorder-dependent quantity $p_0^{(4)}(t=0)$, when combined with the disorder-independence of $p_0^{(2)}(t=0)$, implies at least at short times it does not matter when the disorder averaging is performed. That is, averaging p_0 before calculating $K(t)$ will give the same result as averaging over all $K(t)$ associated with each realization of p_0 . This gives an explicit example of our claim that for short times $K_{\text{avg}}(t) \approx \bar{K}(t)$.

Evaluation of the fourth derivative for p_0 is more involved, but proceeds along a similar route. Generally speaking, note that these derivatives rely on the dynamics of coherences (i.e. off-diagonal elements) in the full density matrix.

$$\begin{aligned} [H, [H, |0\rangle\langle 0| \otimes \hat{I}_B]] &= \gamma_\perp [H, \hat{\tau}^+ \otimes \hat{M}_B^- - \hat{\tau}^- \otimes \hat{M}_B^+] \\ &= \gamma_\perp \left(\hat{\tau}^+ \otimes [H_B, \hat{M}_B^-] - \hat{\tau}^- \otimes [H_B, \hat{M}_B^+] \right) \\ &\quad + \gamma_\perp \gamma_z \left(\hat{\tau}^+ \otimes \{ \hat{M}_B^z, \hat{M}_B^- \} + \hat{\tau}^- \otimes \{ \hat{M}_B^z, \hat{M}_B^+ \} \right) \\ &\quad + \gamma_\perp^2 \left(|0\rangle\langle 0| \otimes (\hat{M}_B^+ \hat{M}_B^- + \hat{M}_B^- \hat{M}_B^+) - |1\rangle\langle 1| \otimes (\hat{M}_B^- \hat{M}_B^+ + \hat{M}_B^+ \hat{M}_B^-) \right) \end{aligned}$$

$$\begin{aligned} [H, [H, |0\rangle\langle 0| \otimes \hat{\rho}_B]] &= [H, |0\rangle\langle 0| \otimes [H_B, \hat{\rho}_B] + \gamma_\perp (\hat{\tau}^+ \otimes \hat{M}_B^- \hat{\rho}_B - \hat{\tau}^- \otimes \hat{\rho}_B \hat{M}_B^+)] \\ &= |0\rangle\langle 0| \otimes [H_B, [H_B, \hat{\rho}_B]] \\ &\quad + \gamma_\perp \left(\hat{\tau}^+ \otimes [H_B, \hat{M}_B^- \hat{\rho}_B] - \hat{\tau}^- \otimes [H_B, \hat{\rho}_B \hat{M}_B^+] \right) \\ &\quad + \gamma_\perp \left(\hat{\tau}^+ \otimes \hat{M}_B^- [H_B, \hat{\rho}_B] - \hat{\tau}^- \otimes [H_B, \hat{\rho}_B] \hat{M}_B^+ \right) \\ &\quad + \gamma_\perp \gamma_z \left(\hat{\tau}^z |0\rangle\langle 0| \otimes [\hat{M}_B^z, [H_B, \hat{\rho}_B]] + \hat{\tau}^+ \otimes \{ \hat{M}_B^z, \hat{M}_B^- \hat{\rho}_B \} + \hat{\tau}^- \otimes \{ \hat{M}_B^z, \hat{\rho}_B \hat{M}_B^+ \} \right) \\ &\quad + \gamma_\perp^2 \left(|0\rangle\langle 0| \otimes (\hat{M}_B^+ \hat{M}_B^- \hat{\rho}_B + \hat{\rho}_B \hat{M}_B^+ \hat{M}_B^-) - |1\rangle\langle 1| \otimes (\hat{M}_B^- \hat{\rho}_B \hat{M}_B^+ + \hat{M}_B^+ \hat{\rho}_B \hat{M}_B^-) \right) \\ &= |0\rangle\langle 0| \otimes [H_B, [H_B, \hat{\rho}_B]] \\ &\quad + \gamma_\perp \left(\hat{\tau}^+ \otimes [H_B, \hat{M}_B^- \hat{\rho}_B] - \hat{\tau}^- \otimes [H_B, \hat{\rho}_B \hat{M}_B^+] \right) \\ &\quad + \gamma_\perp \left(\hat{\tau}^+ \otimes \hat{M}_B^- [H_B, \hat{\rho}_B] - \hat{\tau}^- \otimes [H_B, \hat{\rho}_B] \hat{M}_B^+ \right) \\ &\quad - 2\gamma_\perp \gamma_z \left(\hat{\tau}^+ \otimes \hat{M}_B^- \hat{\rho}_B + \hat{\tau}^- \otimes \hat{\rho}_B \hat{M}_B^+ \right) \\ &\quad + \gamma_\perp^2 \left(|0\rangle\langle 0| \otimes (\hat{M}_B^+ \hat{M}_B^- \hat{\rho}_B + \hat{\rho}_B \hat{M}_B^+ \hat{M}_B^-) - |1\rangle\langle 1| \otimes (\hat{M}_B^- \hat{\rho}_B \hat{M}_B^+ + \hat{M}_B^+ \hat{\rho}_B \hat{M}_B^-) \right) \end{aligned}$$

There will be 6 contributions to the trace:

1. $\gamma_\perp^2 \text{Tr}_B \left((\hat{M}_B^z \hat{M}_B^- + \hat{M}_B^+ \hat{M}_B^z) [H_B, [H_B, \hat{\rho}_B]] \right) = 0$ since $\hat{M}_B^z \hat{\rho}_B = \hat{\rho}_B \hat{M}_B^z = 0$
2. $-\gamma_\perp^2 \text{Tr}_B \left([H_B, \hat{M}_B^+] \left([H_B, \hat{M}_B^- \hat{\rho}_B] + \hat{M}_B^- [H_B, \hat{\rho}_B] \right) + [H_B, \hat{M}_B^-] \left([H_B, \hat{\rho}_B \hat{M}_B^+] + [H_B, \hat{\rho}_B] \hat{M}_B^+ \right) \right)$
3. $\gamma_\perp^2 \gamma_z \text{Tr}_B \left(\{ \hat{M}_B^z, \hat{M}_B^+ \} \left([H_B, \hat{M}_B^- \hat{\rho}_B] + \hat{M}_B^- [H_B, \hat{\rho}_B] \right) - \{ \hat{M}_B^z, \hat{M}_B^- \} \left([H_B, \hat{\rho}_B \hat{M}_B^+] + [H_B, \hat{\rho}_B] \hat{M}_B^+ \right) \right)$
4. $-2\gamma_\perp^2 \gamma_z \text{Tr}_B \left(-[H_B, \hat{M}_B^+] \hat{M}_B^- \hat{\rho}_B + [H_B, \hat{M}_B^-] \hat{\rho}_B \hat{M}_B^+ \right)$
5. $-2\gamma_\perp^2 \gamma_z^2 \text{Tr}_B \left(\{ \hat{M}_B^z, \hat{M}_B^- \} \hat{\rho}_B \hat{M}_B^+ + \{ \hat{M}_B^z, \hat{M}_B^+ \} \hat{M}_B^- \hat{\rho}_B \right) = 8\gamma_\perp^2 \gamma_z^2 \text{Tr}_B \left(\hat{M}_B^+ \hat{M}_B^- \hat{\rho}_B \right)$
6. $\gamma_\perp^4 \text{Tr}_B \left(\{ \hat{M}_B^+, \hat{M}_B^- \} \left(\hat{M}_B^+ \hat{M}_B^- \hat{\rho}_B + \hat{\rho}_B \hat{M}_B^+ \hat{M}_B^- + 2\hat{M}_B^- \hat{\rho}_B \hat{M}_B^+ \right) \right)$

The traces can be evaluated and disorder averaged in the Neel state to give

$$p_0^{(4)} = \underbrace{L\gamma_\perp^2 \left(\frac{W^2}{3} - 16J_z^2 - 4J_\perp^2 + 16J_\perp J_z \right)}_{\boxed{2}} + \underbrace{4L\gamma_\perp^2 \gamma_z J_\perp}_{\boxed{3}} + \underbrace{2L\gamma_\perp^2 \gamma_z (4J_z - J_\perp)}_{\boxed{4}} + \underbrace{4\gamma_\perp^2 \gamma_z^2 L}_{\boxed{5}} + \underbrace{L\gamma_\perp^4 (3L - 4)}_{\boxed{6}}. \quad (\text{F5})$$

Using the couplings for our model, the second derivative of the scalar memory kernel with an initial Neel bath state is given by

$$K^{(2)}(t=0) = - \left(\frac{W^2}{3} + \frac{3}{4} \frac{\gamma}{L} + \frac{3}{4} \frac{\gamma^2}{L} - \frac{3}{4} \frac{\gamma^2}{L^2} \right) \quad (\text{F6})$$